Penn Libraries
UNIVERSITY of PENNSYLVANIA

University of Pennsylvania
ScholarlyCommons

Departmental Papers (EES)   Department of Earth and Environmental Science

3-2012

The Physical Basis for Anomalous Diffusion in Bed Load Transport

Raleigh L Martin
University of Pennsylvania

Douglas J. Jerolmack
University of Pennsylvania, sediment@sas.upenn.edu

Rina Schumer

Follow this and additional works at: http://repository.upenn.edu/ees_papers

Part of the Environmental Sciences Commons, Geomorphology Commons, Hydrology Commons, and the Sedimentology Commons

Recommended Citation

This article has a correction that can be found through the DOI: 10.1029/2012JF002608

The Physical Basis for Anomalous Diffusion in Bed Load Transport

Abstract

Recent studies have observed deviation from normal (Fickian) diffusion in sediment tracer dispersion that violates the assumption of statistical convergence to a Gaussian. Nikora et al. (2002) hypothesized that particle motion at short time scales is superdiffusive because of inertia, while long-time subdiffusion results from heavy-tailed rest durations between particle motions. Here we test this hypothesis with laboratory experiments that trace the motion of individual gravels under near-threshold intermittent bed load transport $(0.027 < \tau^* < 0.087)$. Particle behavior consists of two independent states: a mobile phase, in which indeed we find superdiffusive behavior, and an immobile phase, in which gravels distrained from the fluid remain stationary for long durations. Correlated grain motion can account for some but not all of the superdiffusive behavior for the mobile phase; invoking heterogeneity of grain size provides a plausible explanation for the rest. Grains that become immobile appear to stay at rest until the bed scours down to an elevation that exposes them to the flow. The return time distribution for bed scour is similar to the distribution of rest durations, and both have power law tails. Results provide a physical basis for scaling regimes of anomalous dispersion and the time scales that separate these regimes.

Keywords
anomalous diffusion, bed load transport, sediment transport

Disciplines
Earth Sciences | Environmental Sciences | Geomorphology | Hydrology | Physical Sciences and Mathematics | Sedimentology

Comments
This article has a correction that can be found through the DOI: 10.1029/2012JF002608

The physical basis for anomalous diffusion in bed load transport

Raleigh L. Martin,[1] Douglas J. Jerolmack,[1] and Rina Schumer[2]

[1]   Recent studies have observed deviation from normal (Fickian) diffusion in sediment tracer dispersion that violates the assumption of statistical convergence to a Gaussian. Nikora et al. (2002) hypothesized that particle motion at short time scales is superdiffusive because of inertia, while long-time subdiffusion results from heavy-tailed rest durations between particle motions. Here we test this hypothesis with laboratory experiments that trace the motion of individual gravels under near-threshold intermittent bed load transport ($0.027 < \tau^* < 0.087$). Particle behavior consists of two independent states: a mobile phase, in which indeed we find superdiffusive behavior, and an immobile phase, in which gravels distrained from the fluid remain stationary for long durations. Correlated grain motion can account for some but not all of the superdiffusive behavior for the mobile phase; invoking heterogeneity of grain size provides a plausible explanation for the rest. Grains that become immobile appear to stay at rest until the bed scours down to an elevation that exposes them to the flow. The return time distribution for bed scour is similar to the distribution of rest durations, and both have power law tails. Results provide a physical basis for scaling regimes of anomalous dispersion and the time scales that separate these regimes.

Citation: Martin, R. L., D. J. Jerolmack, and R. Schumer (2012), The physical basis for anomalous diffusion in bed load transport, *J. Geophys. Res.*, *117*, F01018, doi:10.1029/2011JF002075.

1.   Introduction

[2]   One way to quantify sediment flux is by studying the behavior of tracer particles [e.g., *Sayre and Hubbell*, 1965; *Granger et al.*, 1996; *Habersack*, 2001; *Willenbring and von Blanckenburg*, 2010]. Tracer techniques are especially attractive for gravel and coarser sediments, which, because of their size, can be individually tagged and tracked [*Schmidt and Ergenzinger*, 1992; *Chacho et al.*, 1994; *Habersack*, 2001; *McNamara and Borden*, 2004; *Lamarre et al.*, 2005; *Wong et al.*, 2007; *Lamarre and Roy*, 2008]. The statistical behavior of sedimentary tracers is often described [e.g., *Bouchaud and Georges*, 1990] through the scaling diffusion exponent, γ, which relates the growth of variance of particle displacement, σ_x^2, with time interval, δt:

$$\sigma_x^2 = \left\langle \left(\delta x - \overline{\delta x}\right)^2 \right\rangle \propto (\delta t)^{2\gamma}, \qquad (1)$$

where δx is the displacement of an individual particle over δt, $\overline{\delta x}$ is the mean particle displacement for all particles over an interval δt, and the $\langle \rangle$ symbols refer to the ensemble average over all particles. By definition, $\gamma = 0.5$ for normal (Fickian) diffusion, where variance grows linearly with time.

[3]   When $\gamma \neq 0.5$, particle diffusion is "anomalous". Specifically, $\gamma > 0.5$ for superdiffusion, and $\gamma < 0.5$ for subdiffusion. Here we adopt a strictly statistical definition of "diffusion" as measured by the spreading of particles, and use the term without reference to the operative physical processes at all scales. Anomalous sediment tracer diffusion has been observed with sand [*Bradley et al.*, 2010] and gravel [*Nikora et al.*, 2002] tracers. When diffusion is anomalous, statistical moments do not necessarily converge to finite values, thus violating Central Limit Theorem (CLT) assumptions of many sediment transport models. This statistical nonconvergence in turn complicates our ability to infer sediment flux from finite sampling [*Nikora et al.*, 2002; *Ganti et al.*, 2009; *Singh et al.*, 2009; *Bradley et al.*, 2010]. Some anomalous sediment diffusion produces landscape evolution patterns described by fractional advection diffusion equations (FADEs) that require a more generalized version of the CLT, often via flux laws that are nonlocal in space or time [*Stark et al.*, 2009; *Foufoula-Georgiou et al.*, 2010; *Tucker and Bradley*, 2010; *Voller and Paola*, 2010].

[4]   Anomalous diffusion may arise from heavy tails in the distributions of particle steps or waits due to rare extreme events, and can be modeled by FADEs [*Schumer et al.*, 2009]. Alternatively, correlations in particle motion (fractional Brownian motion) may also produce anomalous diffusion, generating a time-varying diffusion exponent [*Mandelbrot and Ness*, 1968]. For example, when particle motions are perfectly correlated, motion is described as "ballistic", and $\gamma = 1$ in equation (1) [*Bouchaud and Georges*, 1990; *Metzler and Klafter*, 2000]. Transition from correlated to uncorrelated particle motion over

[1]Department of Earth and Environmental Science, University of Pennsylvania, Philadelphia, Pennsylvania, USA.
[2]Division of Hydrologic Sciences, Desert Research Institute, Reno, Nevada, USA.

increasing time scales is thus identified as a transition from ballistic to superdiffusion to normal diffusion [*Bouchaud and Georges*, 1990; *Carreras et al.*, 1999; *Metzler and Klafter*, 2000; *Nikora et al.*, 2002; *Marchesoni and Taloni*, 2006; *Kumar et al.*, 2010]. Distinguishing between sources of anomalous diffusion can be a challenge [*Magdziarz et al.*, 2009]. In the case of heavy tails, a direct translation may be made between the tails of the microscale particle step/wait distributions and a fractional advection diffusion equation describing the bulk transport [*Weeks et al.*, 1996; *Schumer et al.*, 2009].

[5] *Nikora et al.* [2002] suggested that the character of anomalous sediment diffusion may change with time scale. In their conceptual model, superdiffusion at short time scales ("local regime") resulted from correlated particle motions arising from particle inertia, and subdiffusion at long time scales ("global regime") resulted from periods of particle immobility (wait times) with a heavy tail. Over medium time scales ("intermediate regime"), *Nikora et al.* [2002] suggested that the character of diffusion may depend on system properties. *Bradley et al.* [2010] observed subdiffusion at this intermediate time scale, while *Nikora et al.* [2002] observed superdiffusion.

[6] While *Nikora et al.* [2002] provided a useful conceptual framework for understanding different scaling regimes in bed load particle diffusion, this framework does not provide specific physical evidence for the sources of anomalous diffusion. The transition between diffusion regimes observed by *Nikora et al.* [2002] is based on an empirical fit between two disparate data sets rather than any kind of physical argument related to durations of particle mobility or immobility.

[7] There are few studies that have directly quantified the physical sources of anomalous sediment transport behavior, i.e., those producing heavy-tailed statistics or correlated motions. A recent experiment by *Hill et al.* [2010] found a heavy-tailed distribution of particle flight lengths. They proposed that this was due simply to grain size heterogeneity, in which individual size classes had exponential flight length distributions, but the superposition of these distributions gave rise to a power law. Other experiments of bed load transport with mixed grain sizes have found only exponential or gamma flight length distributions [*Hassan et al.*, 1991; *Schmidt and Ergenzinger*, 1992; *Habersack*, 2001; *Lamarre and Roy*, 2008; *Lajeunesse et al.*, 2010] or even grain size independence in transport lengths [*Wilcock*, 1997]. Otherwise, physical explanations for anomalous diffusion are still lacking. This lack of physical understanding underlying observed anomalous diffusion in sediment transport has been identified as an important research question in geomorphology [*Foufoula-Georgiou and Stark*, 2010].

[8] Consideration of the mechanics of coarse particle bed load transport may help us to understand the physical basis for anomalous diffusion. Rivers tend to transport gravel and coarser material by bed load transport with bed shear stresses only slightly above the threshold of motion [*Dade and Friend*, 1998], with perhaps a slight increase in transport Shields stress for coarser particles [*Mueller and Pitlick*, 2005]. *Parker* [1978] and *Parker et al.* [2007] showed how river morphology is organized to maintain these threshold conditions during channel-forming floods. In near-threshold

bed load transport for gravel [*Drake et al.*, 1988] and coarser [*Ergenzinger et al.*, 1989; *Schmidt and Ergenzinger*, 1992; *Chacho et al.*, 1994; *Habersack*, 2001] material, particles alternate between mobility and immobility, and always remain close to the bed, either by saltation hops or by rolling/sliding directly along the bed surface [*Drake et al.*, 1988], producing unpredictability in bed particle motion [*Gomez and Phillips*, 1999; *Phillips*, 2006; *Ancey et al.*, 2008; *Singh et al.*, 2009; *Ganti et al.*, 2009; *Ancey*, 2010]. As a result, many predictions of bed load transport are based on a statistical description of sediment motion [*Einstein*, 1950, 1972; *Fernandez Luque and Van Beek*, 1976; *Nakagawa and Tsujimoto*, 1980; *Sekine and Kikkawa*, 1992; *Hu and Hui*, 1996a; *Lisle et al.*, 1998; *Ancey et al.*, 2003, 2008; *Ancey*, 2010; *Lajeunesse et al.*, 2010].

[9] Many of the statistical bed load models referenced above consider particle velocities, the durations of flights (continuous periods of motion) and waits (continuous periods of rest), and rates of entrainment (initiation of particle motion) and distrainment (cessation of particle motion). Statistics of particle motion can in turn be related physically to particle and fluid properties, such as grain size and shear stress [*Bagnold*, 1966, 1973; *van Rijn*, 1984; *Seminara et al.*, 2002; *Francis*, 1973; *Fernandez Luque and Van Beek*, 1976; *Abbott and Francis*, 1977; *Wiberg and Smith*, 1989; *Lee and Hsu*, 1994; *Nino et al.*, 1994; *Lajeunesse et al.*, 2010].

[10] In this paper, we apply physical understanding of particle motion statistics to explain and expand on the conceptual framework for anomalous diffusion of bed load laid out by *Nikora et al.* [2002]. We performed flume experiments to relate the grain-scale physics of gravel bed load to observed anomalous sediment diffusion. In the first set of experiments, we followed continuously moving tracers at short times (<5 s) across a fixed, rough bed, in order to isolate the dynamics of mobile phase particles. In the second set, we followed intermittently moving tracers along a movable bed at long times (up to 30 min) to observe transitions between mobile and immobile phases. We then relate observed transport statistics (particle velocities, flight times, wait times) to scaling and time scales of anomalous diffusion regimes.

2. Methods

[11] We conducted experiments to trace gravel trajectories in a small laboratory flume in the Sediment Dynamics Laboratory at the University of Pennsylvania. The test section length was 200 cm, and the width was 15 cm. In each experiment, water flowed with constant discharge from an upstream inlet; the first 50 cm of the flume were reserved to allow flow to achieve a steady, uniform condition. While we varied water discharge as an experimental variable, all experiments were conducted with Shields stress near critical; i.e., the regime of intermittent motion, as shown in Table 1. The sediments used in all experiments were moderately well sorted natural gravel with $D_{50} = 7.09$ mm, $D_{10} = 5.30$ mm, and $D_{90} = 9.13$ mm, where D_{50}, D_{10}, and D_{90} are the 50th, 10th, and 90th percentiles of grain diameter, respectively. Particle density, $\rho_s = 2650$ kg/m^3, was that of silica.

[12] Considering the time scale difference between continuous motion (at short time scales) and intermittent motion

Table 1. Parameters for Experiments Described in This Paper[a]

Experiment	Q (L/m)	h (m)	Re	$\bar{u}$ (m/s)	τ_*	u_* (m/s)	Bed State	Q_s
F1	57	0.0080	6234	0.78	0.068	0.0884	fixed, 10% slope	One at a time
F2	45	0.0063	4921	0.79	0.053	0.0783	fixed, 10% slope	One at a time
F3	38	0.0060	4156	0.69	0.051	0.0768	fixed, 10% slope	One at a time
F4	30	0.0046	3281	0.71	0.040	0.0675	fixed, 10% slope	One at a time
F5	26	0.0040	2843	0.71	0.034	0.0627	fixed, 10% slope	One at a time
F6	23	0.0038	2515	0.66	0.032	0.0611	fixed, 10% slope	One at a time
F7	21	0.0034	2297	0.68	0.029	0.0577	fixed, 10% slope	One at a time
F8	19	0.0032	2078	0.65	0.027	0.0561	fixed, 10% slope	One at a time
M1	120	0.0215	13124	0.61	0.087	0.0997	movable, ≈ 4.7% slope	1.3 kg/min
M2	120	0.0215	13124	0.61	0.087	0.0997	movable, ≈ 4.7% slope	1.3 kg/min

[a]Q is water discharge, h is mean flow depth, Re is Reynolds number, $\bar{u}$ is mean water velocity, τ_* is Shields stress, u_* is shear velocity, Q_s is sediment discharge.

(at long time scales), two sets of experiments were carried out. For continuous motion, we ran eight tracer experiments, henceforth labeled "F1, F2,…F8." In these experiments, the bed was fixed by gluing random close-packed gravel particles (with the same size characteristics as mobile gravel) to the bottom of the flume, thus preserving the roughness characteristics of a natural movable gravel bed. A fixed bed was used to isolate the dynamics of continuously moving tracer particles while ignoring the exchange of particles between motion and rest. In these experiments, excess shear stress was generally too high for particle rests ever to occur, except for a few distrainments in experiment F8. Thus, the observations provide a representative sampling of the mobile tracer particle population. The fixed-bed cross section had a trapezoidal profile, with a 12 cm width flat central part of the bed, and 1.5 cm width walls sloped at a 45° angle. In all fixed-bed experiments, the longitudinal slope of the bed was set at 10%. The fixed bed was painted white as the background, while tracer grains, fed one at a time in motion from upstream, were red (Figure 1a). A fixed bed has been shown to alter the takeoff angles of saltating particles along the bed and extract less momentum from bed particle collisions [*Abbott and Francis*, 1977], but using a fixed bed offered the advantage of greatly simplifying the particle tracking process.

[13] Four video cameras were mounted along the length of the flume, and captured video of the bed at 30 frames per second and with 0.86 mm spatial resolution. The video covered a bed area of 199 by 15 cm. Using ImageJ, an open source image analysis software developed by the National Institutes of Health, we extracted the trajectories of tracer grains through the flume. The entire trajectories of grains were tracked from their entry into the channel until they stopped moving or exited the channel. An example of tracked trajectories can be seen in Figure 2.

[14] Flow depth was calculated from images of the side of the flume, and mean water velocity, $\bar{u}$, from the known hydraulic geometry. The Reynolds number, calculated as $\bar{u}h/\nu$, where h is mean water flow depth, and kinematic viscosity, $\nu = 10^{-6}$ m²/s, for all experiments, indicates fully turbulent conditions and therefore the expectation of critical Shields similitude for all experiments (Table 1).

[15] We note here the steep bed slope (10%) and extremely shallow flow depths on the order of a particle diameter for the fixed-bed experiments. Bed load transport at such low relative submergence (ratio of flow depth to particle size) occurs only at the extreme of steep, boulder-bedded streams, such as the cascade morphology identified by *Montgomery and Buffington* [1997]. Step pool channel reaches may also exhibit the steep slopes [*Grant et al.*, 1990; *Lenzi*, 2001; *Zimmermann and Church*, 2001; *Chin*, 2002; *Chin and Wohl*, 2005; *Church and Zimmermann*, 2007], supercritical flows [*Whittaker and Jaeggi*, 1982; *Grant et al.*, 1990; *Lenzi*, 2001; *Comiti et al.*, 2009], and near unity relative submergences [*Grant et al.*, 1990; *Zimmermann and Church*, 2001] produced in our experiments.

[16] While most closely representing tracer studies in steep, boulder-bedded streams [e.g., *Schmidt and Ergenzinger*, 1992; *Lamarre and Roy*, 2008], our experiments were not intended to directly reproduce transport conditions in any particular stream morphology. Rather, they were performed to consider the generic process of bed load particle dispersion. As we will show later, dispersion of continuously moving particles is primarily driven by the statistics of particle velocity, which are in turn determined by shear velocity. Needless to say, relative submergence strongly affects the turbulent
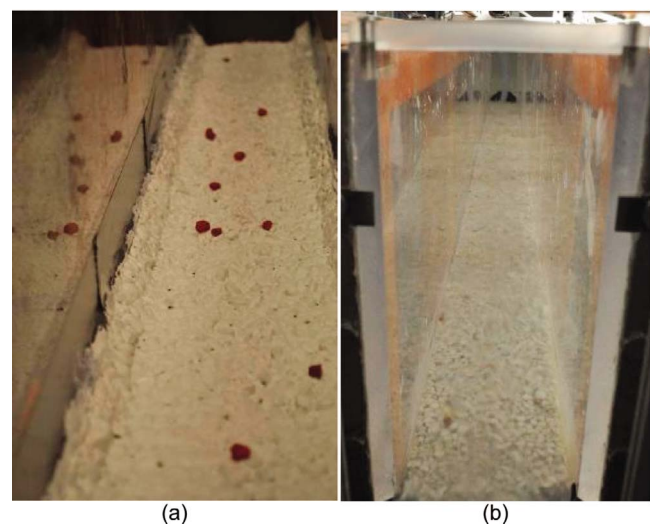

(a)   (b)

Figure 1. The experimental flume, looking upstream. (a) Shown with fixed (white) bed, with a few (red) tracers at rest on the bed. (b) Shown with movable bed. Red tracers are also present here but are more difficult to see, because they are mixed in among the white grains.
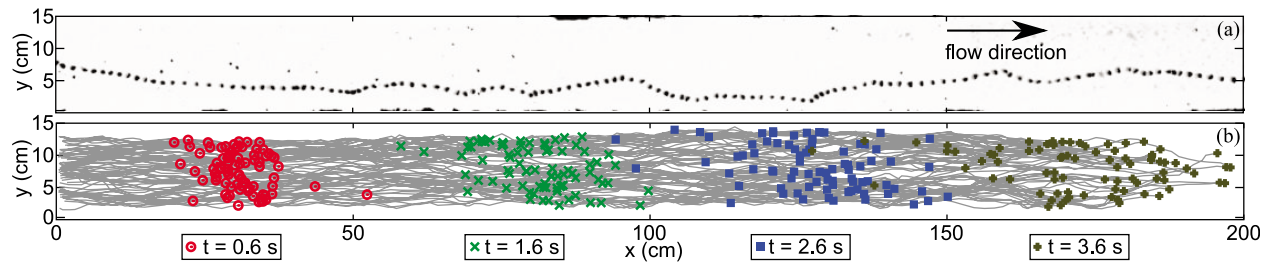
Figure 2. Demonstration of flume particle tracking in experiment F4. (a) Composite image of a single particle trajectory tracked through image processing, showing particle positions at successive 1/30 s intervals. (b) Lines show traces of all trajectories analyzed in experiment. Colored markers show cloud of particle positions at successive 1 s intervals.

stresses and form drag of open channel flows [*Nikora and Goring*, 2001]. For completeness, future experiments could consider particle dispersion under deeper flows.

[17] For intermittent motion at longer time scales, we carried out two movable bed experiments, henceforth labeled "M1" and "M2." In these experiments, the flume was filled with a thick carpet of gravel, and we tracked painted tracers among the overall population of gravel (Figure 1b). Water flowed steadily from upstream as in experiments F1–F8, and gravel was also fed steadily from a hopper (Eriez VFM 15-1-20 Vibratory Feeder) at the upstream end of the flume. Prior to beginning measurements for each movable bed experiment, the steady water and sediment feed was allowed to run for a sufficient length of time to achieve an equilibrium bed slope (about 4.7%) and bed load transport rate (about 1.3 kg/min), so that the rate of sediment entering the flume equaled the rate of sediment exiting. Comparison of the bed surface before and after measurements indicated no discernible armoring for the movable bed experiments, probably because of the narrow range of particle sizes used in the experiments. As the bed particles were not fixed, there was a free interchange of particles between the bed and the bed load layer. Thus, in the movable bed experiments, we tracked particles across all of their entrainment (particle mobilization) and distrainment (particle immobilization) transitions, as well as the duration of waits and flights between these transitions.

[18] In experiment M1, we tracked tracer particles by processing images collected by an array of cameras above the flume, with the same spatial resolution and coverage area as in the F1–F8 experiments. In M2 we tracked particles with photos captured at a 1.32 s interval through the Plexiglas sidewall of the flume, in order to observe the coevolution of bed topography and entrainment/distrainment transitions. Spatial resolution of these photos was 0.05 mm, and photo area was 9.8 mm (horizontal) by 6.5 mm (vertical). Also, in M2, all particles were painted white, and the water was dyed black in order to better track the evolution of bed topography. By differencing between successive image frames, it was possible to isolate distrainment and entrainment events during an individual time step and consider particle wait times in light of bed surface fluctuations.

3. Results

3.1. Fixed-Bed Experiments

[19] Through image analysis of videos captured for experiments F1–F8, we tracked the two-dimensional motion of tracer particles as they traveled along the bed of the flume. In describing particle displacement in the flume, $x = 0$ at the top of the test section and increases downstream, while $y = 0$ at the right bank and increases in the transverse direction (Figure 2). All measurements are described in the reference frame of the flume.

[20] The particle trajectory time series analyses for the fixed-bed experiments are based on tracking tracer particles through the length of the flume. Because of the challenge of following particles through a turbulent water flow in the flume, traces of certain trajectories were incomplete. For consistency, we limit our analyses to those particle trajectories that could be followed through the entire length of the flume. Also, we limit the duration of the particle trajectory

Table 2. Parameters for Fixed-Bed Analysis and Observed Velocity Distributions Measured at Time Interval of $\Delta t = 1/30$ s[a]

Experiment	T (s)	N	τ_*	u_* (m/s)	$\bar{v}_x$ (m/s)	σ_{v_x} (m/s)	$\bar{v}_y$ (m/s)	σ_{v_y} (m/s)	T_c (s)
F1	2.47	58	0.068	0.0884	0.7189	0.147	0.004	0.107	0.043
F2	2.53	55	0.053	0.0783	0.6639	0.140	0.003	0.099	0.052
F3	3.10	50	0.051	0.0768	0.5589	0.128	0.002	0.093	0.041
F4	3.63	81	0.040	0.0675	0.4756	0.113	0.001	0.088	0.065
F5	3.80	65	0.034	0.0627	0.4571	0.106	0.000	0.081	0.049
F6	4.37	48	0.032	0.0611	0.3829	0.098	0.003	0.076	0.056
F7	4.50	43	0.029	0.0577	0.3329	0.091	0.002	0.074	0.073
F8	5.50	12	0.027	0.0561	0.3082	0.084	0.000	0.074	0.073

[a]T is the duration over which trajectories were traced in seconds, N is the number of particles analyzed, τ_* is the dimensionless Shields stress, u_* is shear velocity, $\bar{v}_x$ is the particle mean longitudinal velocity, σ_{v_x} is the standard deviation of longitudinal velocity, $\bar{v}_y$ is the mean transverse velocity, σ_{v_y} is the standard deviation of transverse velocity, T_c is the correlation time scale.
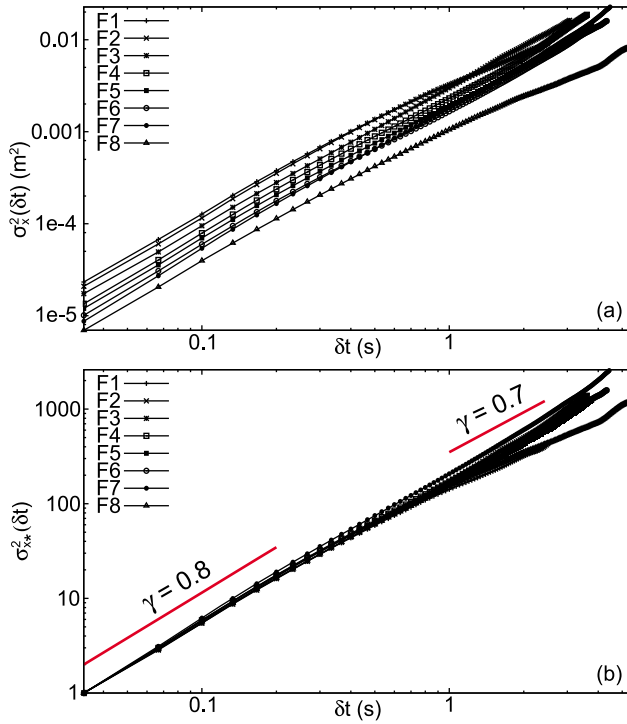
Figure 3. (a) Growth of $\sigma_x^2(\delta t)$, the particle dispersion, versus δt for fixed-bed experiments. (b) Growth of $\sigma_{x*}^2(\delta t)$, the normalized particle dispersion, versus δt. The slopes of the curves decrease slightly with increasing time interval. Linear regression to the mean of the normalized particle dispersion curves over the first 0.2 s gives a dispersion exponent of $\gamma = 0.80$, while $\gamma = 0.70$ for the mean of curves beyond 1 s.

time series to the minimum time for a particle to traverse the entire flume, so that ensemble averages at all time scales will consider the same number of particles. The numbers of particles thus traced (N) and the duration of tracing (T) are provided in Table 2 for each experiment.

3.1.1. Particle Dispersion

[21] As described earlier in equation (1), the particle dispersion can be described by the growth in the variance of particle displacement with time interval. A normalization useful for comparing successive experiments is to divide by the variance at the camera frame rate, $\Delta t = 1/30$ s:

$$\sigma_{x*}^2(\delta t) = \frac{\sigma_x^2(\delta t)}{\sigma_x^2(\Delta t)}, \qquad (2)$$

where $\sigma_{x*}^2(\delta t)$ describes the normalized variance of particle displacement over the interval δt. Note that when we describe dispersion, we are not directly treating a plume of tracers beginning from the same location at exactly the same time. Instead, we consider a "virtual" plume of individually released tracers by setting $t = 0$ for each particle at the instant when it begins its journey at the top of the test section. σ_{x*}^2 for each δt is determined from the ensemble average over all possible time pairs, $N(T - \delta t/\Delta t)$ total. While the number, N, of particles for each experiment is not so large, this method of calculating dispersion ensures averaging over a large number of observations, particularly for small δt.

[22] The longitudinal particle dispersions thus calculated for experiments F1–F8 are shown in Figure 3. In all experiments, the variance exhibits power law growth in both the x and y directions. The power law exponent in the x direction is roughly constant with increasing time interval, but in the y direction (not plotted), the variance growth slows with increasing time interval. This is because of the limitation imposed by the narrow flume width. Because of this spatial limitation, we will focus only on x dispersion in further analysis.

[23] When comparing the nonnormalized dispersions, the variance differs between experiments because of the increased diffusivity of particles under higher flow conditions. However, when normalized, the dispersion curves collapse together. All of the curves appear statistically superdiffusive, with γ significantly greater than 0.5. The dispersion curves show a slight decrease in dispersion exponent with increasing time interval. Linear regression to the mean of the normalized particle dispersion curves over the first 0.2 s gives a dispersion exponent of $\gamma = 0.80$, while $\gamma = 0.70$ for the mean of curves beyond 1 s (Figure 3b). This observed scaling range is close to the range of $\gamma = 0.77 - 0.87$ observed by *Nikora et al.* [2002].

3.1.2. Particle Velocities

[24] Instantaneous longitudinal particle velocities, $v_x(t)$, are determined as the differences between particle displacements, $x(t)$, at successive time steps defined by the camera observation interval of $\Delta t = 1/30$ s:

$$v_x(t) = \frac{x(t) - x(t - \Delta t)}{\Delta t}. \qquad (3)$$

The distributions of longitudinal particle velocities are shown in Figure 4, with velocity statistics (both v_x and v_y) described in Table 2. These distributions describe the collection of all instantaneous velocities of all particles over the duration of each experiment. While the velocity statistics vary among experiments under varying water discharge (and thus shear stress), the distributions of v_x and v_y are essentially Gaussian for all runs, as can be seen for v_x by the normalized curves in Figure 4b. Note that the observed velocities are explicitly tied to the choice of observation interval, Δt. With increasing Δt, we expect velocity variability to decrease.

[25] Mean particle velocities are compared to experimental shear velocities in Figure 5a, where shear velocity is defined as $u_* = \sqrt{\tau_b/\rho}$, and boundary shear stress is determined as the depth slope product, $\tau_b = \rho ghS$. Here, ρ is water density, g is gravitational acceleration, and S is water surface slope. Within the range of our experiments, mean particle velocities, $\bar{v}_x$, appear to be linearly dependent on shear velocity, though with a nonzero x intercept, here calculated to be $u_{*,0} = 0.033$ m/s for a least squares regression. The dependence of particle velocity on shear velocity can be described by the relation:

$$\bar{v}_x = a(u_* - u_{*,0}). \qquad (4)$$

The best fit to our measurements shown in Figure 5a reveals a coefficient of $a = 13.6$.

[26] Many researchers have examined the relationship between particle velocity and shear velocity for bed load.
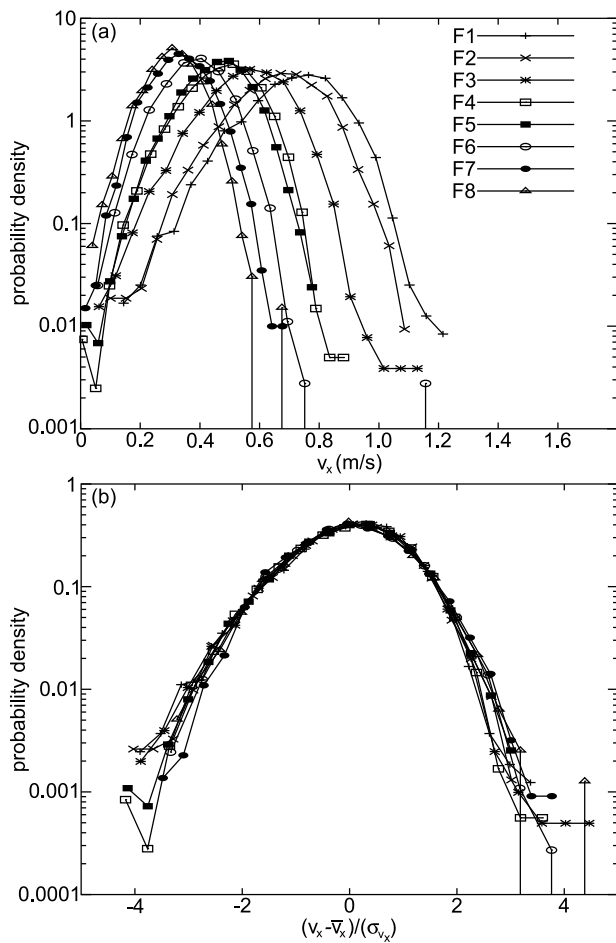
Figure 4. (a) Distribution of longitudinal velocities, v_x (m/s), determined from displacements over 1/30 s intervals. (b) Distribution of normalized longitudinal velocities, $(v_x - \bar{v}_x)/(\sigma_{v_x})$. The curves collapse together toward a common Gaussian profile when normalized.

Published velocity relationships for fixed-bed experiments are shown for comparison in Table 3. All but two studies [*Meland and Norrman*, 1966; *Lee and Hsu*, 1994] reported linear relationships between $\bar{v}_x$ and u_*. Also, for the linear

relationships, all past studies reported a positive value of $u_{*,0}$.

[27] Our observed $a = 13.6$ falls in the range of reported values (except for the study by *Ancey et al.* [2002], which reported an anomalously large value of $a = 35$). As noted by *Abbott and Francis* [1977] and *Lajeunesse et al.* [2010], fixed beds exert less friction resisting particle motion than do movable beds; thus, the observed values of a for movable beds (e.g., $a = 11.6$ [*Fernandez Luque and Van Beek*, 1976]; $a = 8$ [*Sekine and Kikkawa*, 1992]; 6.8–8.5 [*Nino et al.*, 1994]; 4.4 [*Lajeunesse et al.*, 2010]), are usually smaller than for fixed beds. Importantly, the similarity between our particle velocity curves and those of other researchers (both for movable and for fixed beds), supports the dynamic similarity of our particle velocities to those observed in a variety of other systems, particularly those with higher relative submergence.

[28] In the equation of *Bridge and Dominic* [1984], listed in Table 3, $u_{*,0}$ is equated to $u_{*,c}$, the threshold shear velocity for incipient particle motion. Similarly, *Lee and Hsu* [1994] equate the zero intercept for Shields stress, $\tau_* = (u_*^2)/(RgD)$, with the critical Shields stress, $\tau_{*,c}$, for incipient particle motion. ($R = (\rho_s - \rho)/\rho$ is submerged specific gravity.) In other equations [*Fredsøe and Engelund*, 1975; *Hu and Hui*, 1996b], $u_{*,0}$ is smaller than $u_{*,c}$. In the rest of the studies, no interpretation was offered for $u_{*,0}$ in terms of threshold values.

[29] Assuming that $u_{*,0} = u_{*,c}$ gives a threshold Shields stress of $\tau_{*,c} = 0.009$ for our experiments. This is significantly smaller than values typically quoted for turbulent flows, usually around $\tau_{*,c} = 0.05$ for gravel [*Buffington and Montgomery*, 1997]. Our unusually low value of $\tau_{*,c}$ could simply be a consequence of assuming $u_{*,0} = u_{*,c}$. $u_{*,0}$ is effectively a distrainment threshold, i.e., the value to which shear velocity must drop in order to bring an initially moving grain to rest. In line with many past observations [e.g., *Francis*, 1973; *Reid et al.*, 1985; *Drake et al.*, 1988; *Ancey et al.*, 2002], we noticed when setting up our experiments that entrainment of resting grains occurs at a significantly higher Shields stress than distrainment of moving grains. Therefore, $\tau_{*,c}$ would be significantly larger if taken as an entrainment threshold. Indeed, the relations of *Fredsøe and Engelund* [1975] and *Hu and Hui* [1996b] assume values of
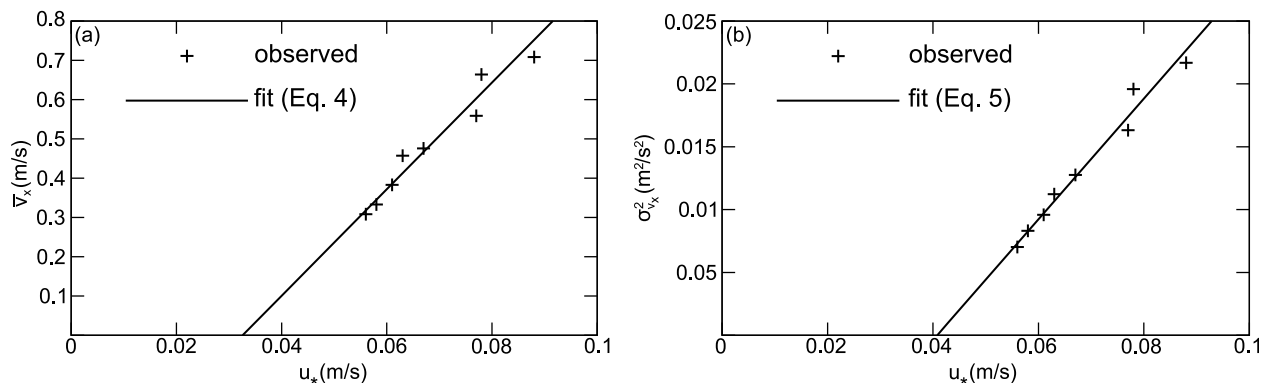

Figure 5. (a) Mean particle velocity, $\bar{v}_x$, versus shear velocity, u_*, for the eight fixed-bed experiments described in this paper. Mean particle velocity, $\bar{v}_x$, increases linearly with u_* according to equation (4), and the x intercept is $u_{*,0} = 0.033$ m/s. (b) Total longitudinal velocity variance, $\sigma_{v_x}^2$, also increases linearly with u_* according to equation (5), with $u_{*,0,\sigma} = 0.041$ m/s.

Table 3. Particle Velocity Versus Shear Velocity Relationships Computed in Various Experiments With a Fixed Rough Bed

Author	Equation	Parameters	Notes
Meland and Norrman [1966]	$\bar{v}_x = 7.05 k^{m-1} D^n (u_* - 0.72 k D^{-n})$	k = roughness length, m and n depend on u_*, D, and k.	Spheres on bed of glass beads experiencing all modes of bed load.
Francis [1973]	$\bar{v}_x = a(u_* - u_{*,0})$	$a = 14.0$ for solitary particles, $a = 14.8$ for particles in a crowd.	Natural particles in saltation only. Equation is our fit to data from *Frances* [1973, Table 5].
Fredsøe and Engelund [1975] (cited by *Middleton and Southard* [1977])	$\bar{v}_x = a(u_* - u_{*,0})$	$a = 10$. $u_{*,0} = 0.7 u_{*,c}$.	Based on data from *Francis* [1973], *Fernandez Luque* [1974], and *Meland and Norrman* [1966].
Abbott and Francis [1977]	$\bar{v}_x = a(u_* - u_{*,0})$	$a = 14.3$ for spheres; $a = 13.5 - 13.85$ for angular grains.	Natural particles experiencing all modes of transport (i.e., rolling, saltation, and suspension).
Bridge and Dominic [1984]	$\bar{v}_x = a(u_* - u_{*,0})$	$a = 6 - 14$. Authors claim a should increase with shear stress. $u_{*,0} = u_{*,c}$.	Theoretical derivation for all modes of bed load based on solving equations of motion.
Lee and Hsu [1994]	$\bar{v}_x = a(\tau_* - \tau_{*,c})^{0.174}$	$a = 11.53$.	Natural particles in saltation only. Our own fit to authors' data for 1.36 mm sand gives $\bar{v}_x = a(u_* - u_{*,0})$ with $a = 11.85$.
Hu and Hui [1996b]	$\bar{v}_x = a(u_* - u_{*,0})$	$a = 11.9$; $u_{*,0} = 0.44 u_{*,c}$.	Natural particles experiencing all modes of bed load.
Ancey et al. [2002]	$\bar{v}_x = a(u_* - u_{*,0})$	$a = 35$.	Spheres on bed of glass beads experiencing all modes of bed load.
This paper	$\bar{v}_x = a(u_* - u_{*,0})$	$a = 13.6$.	Natural particles experiencing all modes of bed load.

$u_{*,c}$ based on an entrainment threshold, giving $u_{*,0} < u_{*,c}$ (Table 3).

[30] Alternatively, our low value of $\tau_{*,c}$ could be a consequence of experimental conditions. As demonstrated for particle velocities, a fixed bed tends to exert less friction on particles than a movable bed, which could perhaps depress $\tau_{*,c}$. Also, $\tau_{*,c}$ tends to decrease as grain size increases relative to bed pocket size, because of greater protrusion and exposure of coarse grains, and values as low as $\tau_{*,c} = 0.01$ have been observed [*Fenton and Abbott*, 1977; *Andrews*, 1983; *Buffington et al.*, 1992; *Wilcock*, 1998]. In our experiments, the white paint covering the fixed bed may have filled in some pockets and caused greater protrusion of resting tracers, thereby decreasing $\tau_{*,c}$. In their exhaustive compilation of incipient motion studies, *Buffington and Montgomery* [1997] note that differences in channel roughness, slope, and sorting produce large variations in observed $\tau_{*,c}$.

[31] Finally, concavity of the u_* versus $\bar{v}_x$ relationship, as observed by *Meland and Norrman* [1966] and *Lee and Hsu* [1994], could produce a greater value of $u_{*,0}$, though Figure 5a indicates no deviation from a linear relationship in our experiments. In fact, when we examined the data for 1.36 mm sand in the experiments of *Lee and Hsu* [1994], we found a linear relationship with $a = 11.85$, matching many of the other quoted experiments.

[32] In addition to $\bar{v}_x$, we can also relate σ_{v_x} to u_*. When we plot $\sigma_{v_x}^2$ versus u_* (Figure 5b), we find a linear relation similar to that for $\bar{v}_x$ versus u_*:

$$\sigma_{v_x}^2 = a_\sigma (u_* - u_{*,0,\sigma}). \qquad (5)$$

In this case, $u_{*,0,\sigma} = 0.041$ m/s, slightly larger than $u_{*,0}$ computed from mean particle velocities, while $a_\sigma = 0.48$ m/s. σ_{v_x} also grows linearly with $\bar{v}_x$.

3.1.3. Particle Velocity Autocorrelation

[33] Because particles possess momentum, successive velocities are correlated over short times. This is quantified by calculating the autocorrelation of grain velocities, R_{v_x}. The velocity autocorrelation is described as a function of time lag, τ, and can range in value from 1 (perfectly correlated) to -1 (perfectly anticorrelated).

[34] For each of the F experiments, we computed the $R_{v_x}(\tau)$ curves for each individual particle trajectory. We focus here only on the longitudinal (x) component of the particle motion, as the narrow width of the channel contributes a spurious anticorrelation for y velocities. To extract the overall particle behavior, we ensemble averaged the $R_{v_x}(\tau)$ curves for all of the particles in each experiment. The resulting ensemble averaged autocorrelation curves, $\langle R_{v_x}(\tau) \rangle$, are shown in Figure 6.

[35] Despite differences in Shields stress among the eight experiments, the longitudinal velocity autocorrelations display a similar rapid exponential decay for all experiments. We can compute a characteristic *e*-folding correlation time scale, T_c, that fits an exponential to the observed autocorrelation curve, i.e.:

$$R_{fit}(\tau) = e^{-\tau/T_c}. \qquad (6)$$

The correlation time scale was calculated by fitting to the autocorrelation curves for time lags up to 1/3 s (the approximate time when all of the autocorrelation curves go to zero) for each data set. The correlation time scales for the eight fixed-bed experiments are given in Table 2. There is a very weak trend of increasing correlation time scale with decreasing shear velocity of the flow, though this trend may be statistically insignificant ($R^2 = 0.60$). The mean correlation time scale among the eight fixed-bed experiments is $T_c = 0.056$ s. The importance of correlation time scale and its relation to particle inertia will be discussed later.
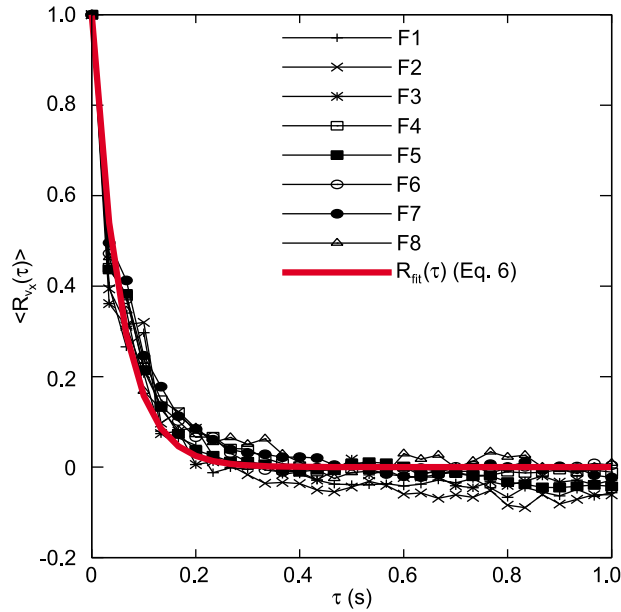
Figure 6. Ensemble-averaged longitudinal velocity auto-correlation curves, $\langle R_{v_x}(\tau)\rangle$. The autocorrelations are similar for all experimental runs, despite differences in Shields stress. An exponential of form $R_{fit}(\tau) = e^{-\tau/T_c}$ (equation (6)) was fit to the means of the $\langle R_{v_x}(\tau)\rangle$ curves for the eight experiments. The characteristic correlation time, T_c, describes the rate of decay of the exponential. T_c varies slightly among experiments (Table 2). The mean for all experiments is $T_c = 0.056$ s.

3.2.　Movable Bed Experiments

3.2.1.　Particle Flights

[36] We measured the duration and length of particle flights, from the moment of entrainment to the moment of distrainment, for 102 particles in experiment M1. Operationally, a resting particle was considered entrained when it moved a complete particle diameter, while a mobile particle was considered distrained when it failed to move more than one grain diameter within a second. Of the 102 particles tracked, only 2 particles traveled the entire length of the flume without becoming distrained; thus, the results can be considered robust for describing the distributions of flight durations and lengths. These distributions are shown in Figure 7. The mean flight time, T_f, is 1.52 s, the mean flight length, L_f, is 0.148 m, and both distributions are thin tailed. Furthermore, the flight times appear to closely follow an exponential distribution. The distribution of flight lengths is more uncertain, possibly but not convincingly of exponential character.

3.2.2.　Particle Wait Times

[37] Particle wait time is the duration of time between distrainment of a grain and reentrainment of that grain. We tracked particle wait times by two methods. In experiment M1, we tracked a total of 243 red tracers from overhead images of the flume. Of these, we measured wait times of less than 30 min for 236 particles, while the other 7 particles were never reentrained after 30 min of waiting. The wait
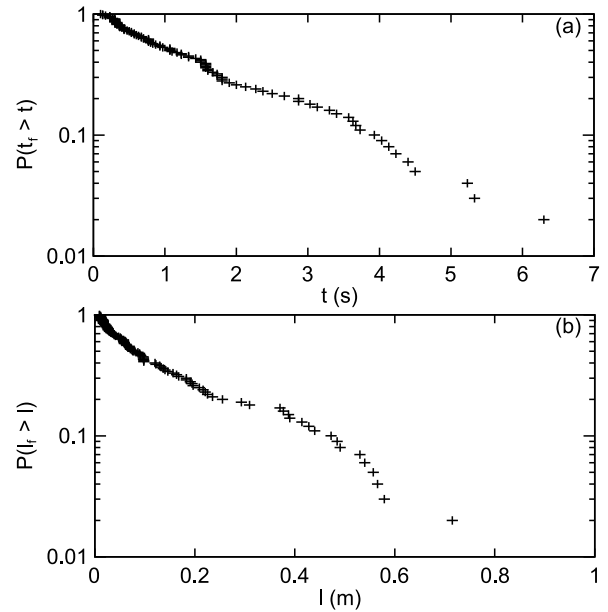

Figure 7. (a) Exceedance probability of flight durations and (b) lengths for 102 particles tracked in experiment M1. The observed distributions strongly suggest an exponential distribution of flight durations and more weakly suggest exponential flight lengths. Mean flight time, T_f, is 1.52 s, and mean flight length, L_f, is 0.148 m.

times were sorted to provide the exceedance probability of wait times, $P(t_w > t)$, where t_w is the particle wait time.

[38] The observed wait time distribution for experiment M1 displays a power law tail (Figure 8). The power law tail has the form:

$$P(t_w > t) \sim t^{-\alpha}, \quad t > T_t. \tag{7}$$

Presumably, because of the finite size of the flume, there should be an upper limit truncation of the wait time distribution; however, the duration of our experiments was insufficient to achieve this supposed wait time truncation. To determine the tail parameter, we used the method of *Nuyts* [2010] for truncated data sets. Taking $T_t = 37$ s as the
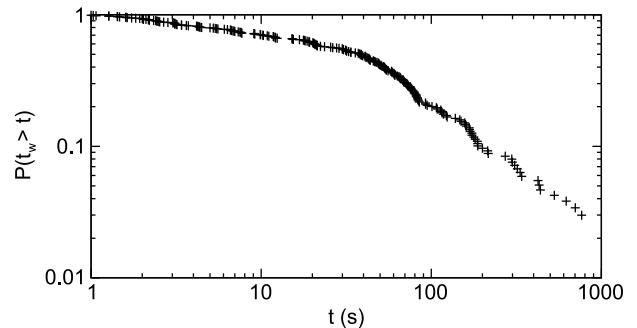

Figure 8. Exceedance probability of particle wait times observed in experiment M1. The tail parameter, $\alpha = 0.85$, where $P(t_w > t) \sim t^{-\alpha}$, was determined by the method of *Nuyts* [2010]. The chosen cutoff time, $T_t = 37$ s, maximizes the fit to the observed data.

cutoff time maximizing the fit to the observed tail, this method produces a tail parameter of $\alpha = 0.85$ for the wait time distribution (equation (7)).

4. Discussion

4.1. Inertial Particle Dynamics and Short-Time Superdiffusion

4.1.1. Correlation Time Scale

[39] The longitudinal velocity autocorrelation curves described above show that particles retain an exponentially decaying memory of their recent motion, with T_c roughly demarcating a transition between correlated and uncorrelated motion. Past studies have demonstrated three primary sources of positively autocorrelated particle velocities in turbulent fluids: (1) hydrodynamic source, due to coordinated fluid motion in turbulent eddies; (2) boundary source, due to confinement of a particle by bounding surfaces or a harmonic potential field; and (3) particle inertial source, due to ballistic motion of particles [*Snyder and Lumley*, 1971; *Clercx and Schram*, 1992; *Elghobashi and Truesdell*, 1992; *Li et al.*, 2010; *Huang et al.*, 2011].

[40] Turbulent velocity fluctuations have been observed to affect bed load gravel transport on time scales of order 0.5 s [*Nelson et al.*, 1995; *Buffin-Belanger and Roy*, 1998]. This is longer than the observed correlation time scale in our experiments, but still of a reasonable enough duration to potentially cause coordinated particle motion in our experiments.

[41] We observed slightly anticorrelated transverse particle velocities, v_y, in our experiments, likely due to the confining presence of channel boundaries. However, no such anticorrelation was observed for longitudinal particle velocities, v_x (Figure 6). Furthermore, the distributions of v_x displayed no differences along the transverse (y) bed direction, suggesting a negligible effect of channel boundaries on autocorrelation of v_x.

[42] The time scale of particle velocity correlations due to particle inertia is related to the time for a particle to respond to fluctuations in fluid drag. Through a simple momentum balance for spherical particles, *Elghobashi and Truesdell* [1992] found this time, T_i, to be:

$$T_i = \frac{4}{3} \frac{\rho_s}{\rho} \frac{D}{C_d} \left(\frac{1}{u - v_x} \right), \quad (8)$$

where $u - v_x$ is the slip velocity (the difference between fluid and particle velocities) and C_d is the drag coefficient. For our experiments, $\rho_s = 2650$ kg/m^3, $\rho = 1000$ kg/m^3, and $D = D_{50} = 7.09$ mm. Assuming a value of $C_d = 1$ for angular particles [*Ferguson and Church*, 2004], and taking $u = \langle \bar{u} \rangle = 0.71$ m/s and $v_x = \langle \bar{v}_x \rangle = 0.49$ m/s as the average of mean water and grain velocities, respectively, across all experiments, we calculate $T_i = 0.11$ s.

[43] This calculated T_i is double the value of $T_c = 0.056$ s estimated from the autocorrelation curves. Some of this discrepancy may be explained by uncertainty in the drag coefficient, and some by the variability in particle and fluid velocities away from the mean value. Future experiments with various particle sizes/densities and bed configurations would provide better evidence for an inertial time scale (or other sources of particle velocity correlation).

4.1.2. Inertia and Superdiffusion

[44] The presence of inertially driven velocity correlations at short time scales suggests a cause for observed superdiffusion. To explore this idea, we treat particle velocity as an autoregressive process, wherein the velocity at each time step combines a contribution of past velocity with a stochastic contribution, as follows:

$$v_t = r v_{t-1} + \xi_t. \quad (9)$$

v_t is the longitudinal particle velocity at time t, and v_{t-1} is the velocity at the previous time step with duration Δt. The r term describes the lag-Δt autocorrelation and is determined from the correlation time scale, T_c, as: $r = e^{-\Delta t/T_c}$. ξ_t is an independent and identically distributed random noise term related to stochastic fluctuations in fluid, bed, and interparticle interaction effects on particle velocity.

[45] We define the displacement of a particle within a single time step as a "step":

$$s_t = v_t \Delta t. \quad (10)$$

[46] The cumulative particle displacement is just the sum of individual steps:

$$x_t = \sum_{i=1}^{t} s_i, \quad (11)$$

and $x_0 = 0$ for all particles.

[47] As described earlier, particle longitudinal velocities measured over $\Delta t = 1/30$ s are normally distributed with mean, $\bar{v}_x$, and standard deviation, σ_{v_x} (Table 2). Since velocities are normally distributed, the distribution for the noise term, ξ_t, is also normal:

$$f_\xi = \mathcal{N}\left(\mu_\xi, \sigma_\xi \right). \quad (12)$$

To ensure constant velocity statistics through time, we compute the noise mean and standard deviation as the uncorrelated portion of a step:

$$\mu_\xi = \bar{v}_x \Delta t (1 - r), \quad (13)$$

$$\sigma_\xi = \sigma_{v_x} \Delta t \sqrt{1 - r^2}. \quad (14)$$

[48] Substituting equations (10) and (12) into equation (9), we describe the autoregressive model in terms of step displacements:

$$s_t = r s_{t-1} + \mathcal{N}\left(\mu_\xi, \sigma_\xi \right), \quad (15)$$

with initial step size, $s_1 = \mathcal{N}(\bar{v}_x \Delta t, \ \sigma_{v_x} \Delta t)$.

[49] We are interested in determining the growth of longitudinal displacement variance, $\sigma_{x,t}^2$, with time. Based on equation (15) and utilizing the properties of expected values and covariance, we derive $\sigma_{x,t}^2$ in Appendix A:

$$\sigma_{x,t}^2 = \sigma_{s_x}^2 \left(t + 2 \sum_{i=1}^{t-1} r^i (t - i) \right), \quad (16)$$

where σ_{s_x} is the step standard deviation, $\sigma_{s_x} = \Delta t \sigma_{v_x}$.
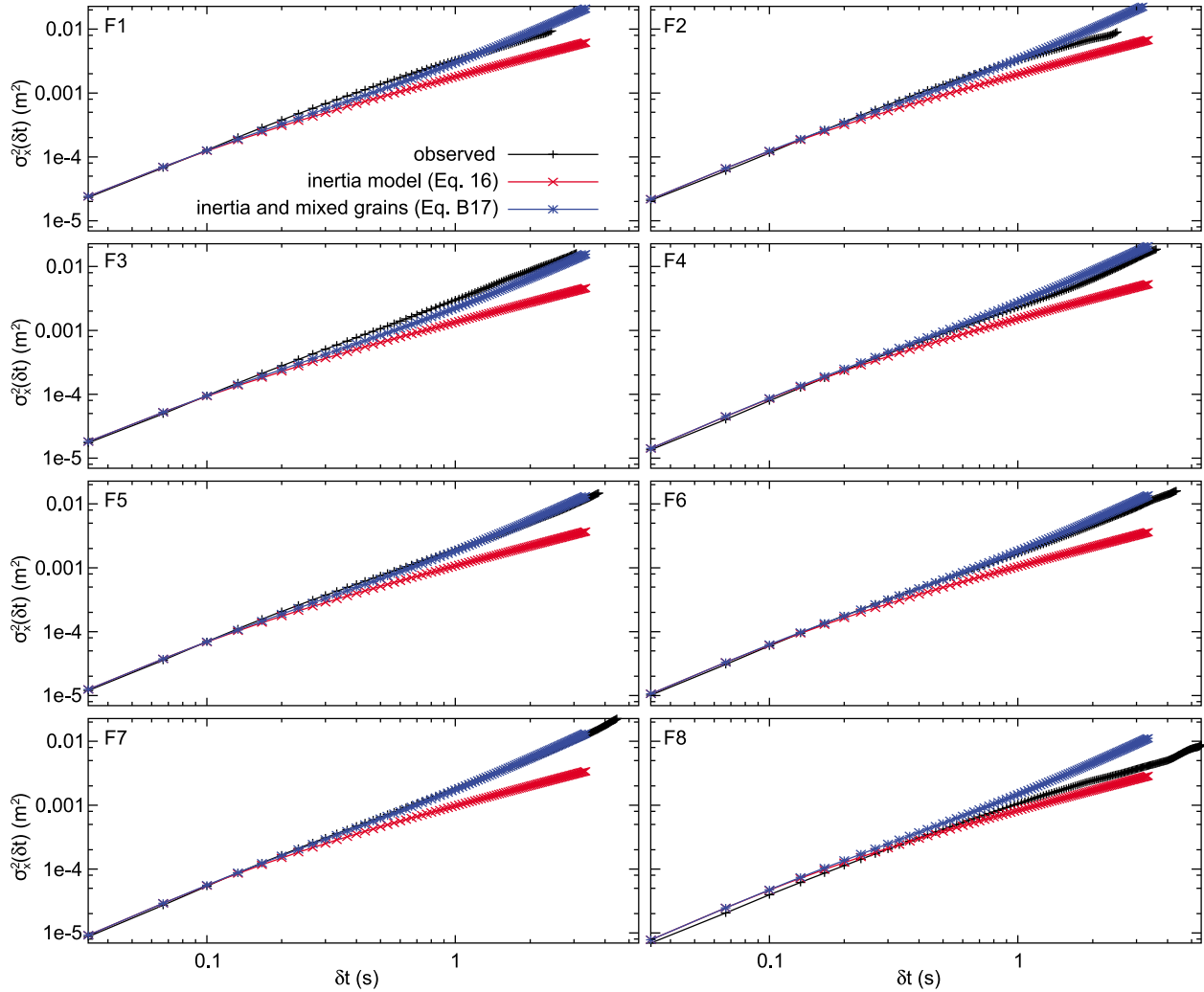
Figure 9. Comparison of particle dispersions for observed tracers, particle inertia autoregressive model (equation (16)), and autoregressive model incorporating mixed grains (equation (B17)) with $\sigma_{v_g}^2/\sigma_{v_x}^2 = 0.015$ (i.e., 1.5% of velocity variance explained by particle heterogeneity). Plots correspond to individual fixed-bed experiments (F1–F8).

[50] Notice in equation (16), the second term on the right hand side describes the expected departure from linear variance growth, and thus the degree of diffusion anomaly. With an increasing value of t, the size of the anomaly gradually decreases relative to the linear variance growth contribution. Thus, at large times, the dispersion gradually converges to normal diffusion, with the rate of convergence dependent on T_c (since $r = e^{-\Delta t/T_c}$).

[51] Using grain motion parameters from Table 2, the autoregressive theory of equation (16) is compared to the observed dispersions in Figure 9. At short times, the theory closely reproduces the observed dispersion in all the runs. In fact, even at times significantly longer than T_c, the effect of inertia still seems to be significant in generating superdiffusion. However, at longer times, the theoretical rate of dispersion gradually declines as the inertial effect wears off. In contrast, the observed dispersion continues to grow at a near constant rate for long times.

[52] What could account for this discrepancy? We think it may be related to grain heterogeneity. While the grain population is well sorted, slight differences among grains mean that some move a bit faster than others over the long term. We can treat this by partitioning fluctuations in particle velocities between those of origin external to an individual grain (i.e., due to turbulence and bed roughness) and those associated with grain heterogeneity:

$$\sigma_{v_x}^2 = \sigma_{v_e}^2 + \sigma_{v_g}^2, \tag{17}$$

where $\sigma_{v_x}^2$ is the total longitudinal velocity variance, $\sigma_{v_e}^2$ is the variance associated with external fluctuations, and $\sigma_{v_g}^2$ is the variance associated with grain heterogeneity.

[53] Reframing the model described in equation (15) to include this partitioning of velocity variance, we develop a more refined model of particle dispersion, which is described in Appendix B. Adopting a value of $\sigma_{v_g}^2/\sigma_{v_x}^2 = 0.015$, i.e., 1.5% of the velocity variability due to grain

heterogeneity, we obtain the modified result shown in Figure 9. At short times, the grain velocity heterogeneity is negligible compared to grain inertia, so the inertial effect predominates. However, at longer times, the magnitude of differences among grains increases in importance, causing the autoregressive model with grain heterogeneity to diverge from the autoregressive model without heterogeneity. Indeed, this model closely reproduces the observed particle dispersion for all runs except for F8, for which the sample size was very small.

[54] While offering a potential explanation for the deviation of observed dispersion from our simple autoregressive model, our autoregressive model with grain heterogeneity is not based on any direct observation of differing particle characteristics. Indeed, our model parameter of $\sigma_{v_g}^2 / \sigma_{v_x}^2 = 0.015$ is simply tuned to match observed dispersion. To obtain a confirmation that the autoregressive model with grain heterogeneity is valid, we would need to measure mean velocities of individual particles over distances much longer than our flume to ensure statistical convergence, then compare the distribution of observed velocities to that for a completely uniform mixture of particles.

[55] The scaling of particle velocity statistics does, however, offer strong evidence for the insufficiency of the simple autoregressive model. The variances in particle velocities, shown for example in Figure 4, are explicitly tied to the averaging interval, here $\Delta t = 1/30$ s. We expect the variance of longitudinal particle velocities, $\sigma_{v_x}^2$, to decrease with increasingly large calculation time interval. However, the exact scaling of $\sigma_{v_x}^2$ with time interval depends on correlations among successive velocities. For example, if successive velocities were completely uncorrelated, by the Central Limit Theorem (CLT) we would expect velocity variance to decline with the inverse of number of time steps sampled. Because successive velocities are correlated, we expect velocity variance to decline more slowly than this.

[56] In Appendix C, we predict how velocity variance, $\sigma_{v_x}^2$, should scale with sampling interval for completely uncorrelated motion (equation (C1)), for inertially correlated motion (equation (C2)), and for inertially correlated motion with grain heterogeneity (equation (C3)). In Figure 10, we show the observed scaling of $\sigma_{v_x}^2$ versus measurement time interval for the eight fixed-bed experiments, and compare this to the predicted $\sigma_{v_x}^2$ scaling for these three cases. Including inertia slightly slows the decline of $\sigma_{v_x}^2$ compared to for uncorrelated motion, but the effect is insufficient to explain the observed $\sigma_{v_x}^2$ scaling. Once grain heterogeneity is included, however, the $\sigma_{v_x}^2$ scaling agrees much better with observations.

[57] Despite the lack of directly applicable data, the agreement of the observed particle dispersion and velocity variance scaling with predictions strongly supports the dispersion model combining grain inertia and heterogeneity. In summary, the inertially driven autocorrelation in velocity determines the correlation time scale, explaining part of the growth in displacement variance. Invoking grain heterogeneity explains the convergence of velocity variance to a nonzero value over long averaging times, and also further helps to explain anomalous displacement variance growth well beyond the correlation time scale.

4.2. Flight Length and Time Distributions

[58] We observed an exponential distribution of flight times, suggesting that distrainment of moving particles along a bed of loose gravel is a memoryless process with probability of distrainment over a time interval related to duration of the time interval only. Flight lengths are also suggestive of an exponential distribution. Our observations are supported by documented exponential- or gamma-distributed particle flight lengths in past studies [*Hassan et al.*, 1991; *Schmidt and Ergenzinger*, 1992; *Habersack*, 2001; *Hill et al.*, 2010; *Lamarre and Roy*, 2008; *Lajeunesse et al.*, 2010]. *Lajeunesse et al.* [2010] tracked the length and duration of particle flights under a variety of hydraulic conditions. Using a poorly sorted lognormal distribution of particles, *Hill et al.* [2010] observed a power law distribution of flight lengths, but ascribed this not to the transport dynamics (individual grain size populations showed exponential flight length distributions), but rather to the presence of a lognormal distribution of grain sizes. Observations by *Schmidt and Ergenzinger* [1992] and *Lajeunesse et al.* [2010] support the notion that flight length depends on particle shape and diameter. In particular, *Lajeunesse et al.* [2010] found that the mean flight times scale with a characteristic particle settling time, which determines the frequency of bed contacts and potential distrainments.

[59] The flight time sets an important constraint on anomalous diffusion regimes. When observing bed particle dispersion over intervals shorter than the characteristic flight time, T_f, one will observe grains mostly in continuous motion. In this case, the dispersion theory described above, combining particle inertia and grain heterogeneity, will produce superdiffusion. However, at times longer than T_f, the rest intervals between successive particle hops should strongly influence particle dispersion.

[60] *Nikora et al.* [2002] predicted from the intersection of two empirical data sets that transition from superdiffusion at short times to subdiffusion at long times should commence when $t u_* / D \approx 15$. Taking the mean flight time, T_f, as the predicted transition time to superdiffusion, we get $T_f u_* / D = 21.3$, close to the empirical prediction of *Nikora et al.* [2002]. Because of the limited length of our flume, we could not test this prediction directly in our experiments.

4.3. Physical Meaning of Wait Times

[61] We have noted the presence of a power law tail in wait times, but where does it come from? For a resting grain to become reentrained, two conditions must be satisfied: (1) sufficient shear stress must be applied to mobilize grains in the section of bed where a particle is residing, and (2) the particle must be exposed on the surface of the bed. Soon after a particle has been distrained (i.e., for short wait times), it is likely to remain exposed to the flow, so only condition 1 limits reentrainment. Thus, we would expect the wait time distribution at short times to be dominated by surface transport patterns. *Drake et al.* [1988] followed collective particle motion on the bed of a gravel stream, and found that these motions tend to aggregate in "sweep-transport events," randomly distributed localized transport events driven by turbulent velocity fluctuations. However, at long times, reentrainment dynamics will be dominated by
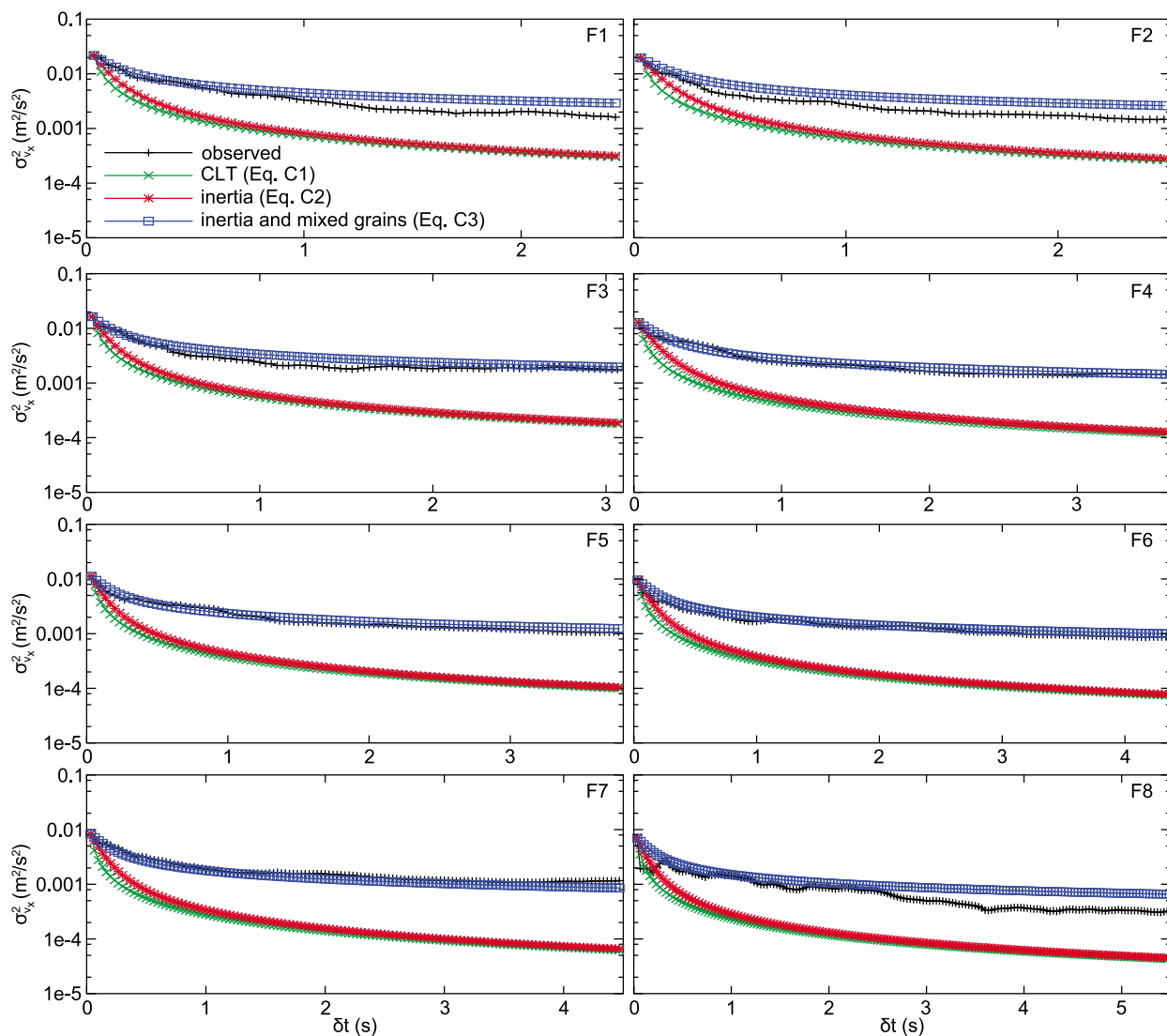
Figure 10. Scaling of velocity variance, $\sigma_{v_x}^2$, with measurement interval, δt. Observed scaling of $\sigma_{v_x}^2$ with δt is compared to predictions for uncorrelated motion (CLT; see also equation (C1)), particle inertia auto-regressive model (inertia; see also equation (C2)), and autoregressive model incorporating grain heterogeneity (inertia and mixed grains; see also equation (C3)). Including inertia slightly slows the decline of $\sigma_{v_x}^2$ compared to uncorrelated motion, but the effect is insufficient to explain the observed $\sigma_{v_x}^2$ scaling. Once grain heterogeneity is included, however, the $\sigma_{v_x}^2$ scaling agrees much better with observations. Plots correspond to individual fixed-bed experiments (F1–F8).

the burial and reemergence of grains by scour as particles interact with neighboring grains.

[62] In experiment M2, we tracked 398 particles on the sidewall of the flume, of which we were able to measure wait times of less than 60 min for 392 particles. The distribution of M2 wait times is shown in Figure 11. By tracking from the sidewall, we could also look at changes in bed topography corresponding to entrainment and distrainment of individual grains. Within the images captured for the experiment, areas occupied by grains appeared as white, while water appeared as black. This strong contrast made it possible to determine the bed surface in each frame, as shown in Figure 12. Bed profiles were captured every 1.32 s for a total of about 90 min.
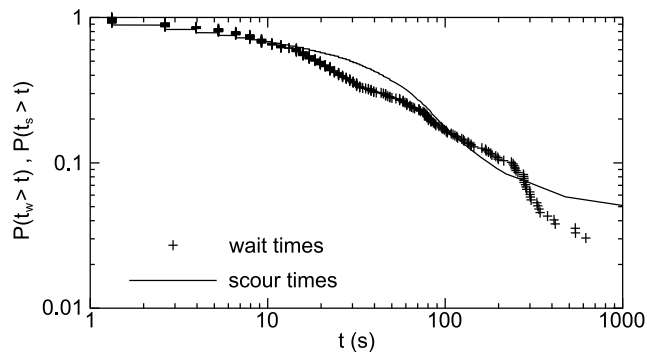

Figure 11. Comparison of wait time (t_w) and scour time (t_s) distributions for experiment M2.
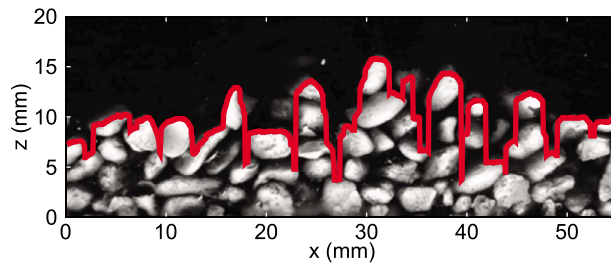
Figure 12. Image of gravel bed from side of flume. Flow is from left to right, and image has been rotated by an angle of $\tan^{-1}(4.7\%)$, corresponding to the mean bed slope. The bed profile marked in red was determined by thresholding in image analysis. Dark spaces appear between particles because their sphericity prevents them from touching at the sidewall where the image is captured.

[63] To understand the coevolution of bed topography with particle wait times, we considered the distribution of scour times of the bed surface. Looking at a single longitudinal position, x, along the bed, the elevation, z, at this position will fluctuate up and down as particles become entrained and distrained. Fluctuations in bed topography are highly irregular, occurring at a range of time scales, from short bursts of intense activity to long periods of quiescence.

[64] Considering this range of bed fluctuations, the bed scour time, $t_s(x, t_0)$, at position x from starting time t_0 is defined as:

$$t_s(x, t_0) = \min(t > t_0 : z(x, t) < z(x, t_0)). \qquad (18)$$

The scour time describes the time until the bed gets reeroded to a certain initial starting position. Because grains are only entrained from the surface of the bed, the bed must scour to at least the top of the grain in order for it to become reentrained (though sufficient shear stress is still required to actually mobilize the particle).

[65] We picked 10000 random positions and times on the bed, and measured the scour times to estimate the distribution of scour times in experiment M2. This distribution is shown in Figure 11, along with the distribution of wait times measured in experiment M2. The scour time distribution mostly describes the observed wait time distribution. Note that the scour time distribution does not converge to zero in the tail, because there are a significant number of bed positions for which the bed never scoured back to the initial position. Presumably, given the limited system size, there must be a maximum time truncation on the power law tail of the wait time distribution, but we did not reach this time in our experiments.

[66] We note here that, because the sidewall interacts with particles to affect their motion, the wait time distribution is somewhat different here than the overall distribution of wait times documented in experiment M1. In particular, the shorter wait times from the sidewall perspective indicate that perhaps the sidewall somewhat decreases the stability of deposited particles. Nonetheless, the presence of a power law tail (here $\alpha = 0.68$ for the power law tail starting at $t_w = 13.2$ s), indicates the rough equivalence of the wait time distributions in experiments M1 and M2.

4.4. Long-Time Anomalous Diffusion

[67] We could not directly measure particle dispersion beyond a few seconds, but our data suggest the potential for anomalous diffusion over long times. The fact that particle flights are thin tailed while particle waits are heavy tailed suggests that the dynamics of wait times should dominate the particle dispersion behavior. Transport processes with thin-tailed flights and heavy-tailed waits may be described by a time-subordinated fractional advection diffusion equation (tFADE) and should experience subdiffusion for $\alpha < 1$ [*Schumer et al.*, 2009]. On the other hand, *Weeks et al.* [1996] described how the net advection of particles may cause superdiffusive particle spreading, despite heavy-tailed wait times.

[68] Taking particle flight times as thin tailed and waits as heavy tailed with decay exponent $\alpha = 0.85$ from the M1 experiments, the expected long-time diffusion scaling exponent for symmetric random walks is $\gamma = \alpha/2 = 0.43$ (slightly subdiffusive), whereas for the asymmetric random walks described by *Weeks et al.* [1996] it is $\gamma = \alpha = 0.85$ (strongly superdiffusive). Since there is net downstream advection of particles in a river, particle motion is best described by an asymmetric random walk, thus predicting long-time superdiffusion. However, *Weeks et al.* [1996] noted that convergence to the limiting diffusive regime can take a very long time; in the interim, when heavy-tailed waits dominate over particle advection, subdiffusion could be possible (thus supporting the observations of *Nikora et al.* [2002] who found $\gamma = 0.33$ for long-time longitudinal particle diffusion for the bed load data of *Drake et al.* [1988]). Perhaps the time truncation of heavy-tailed waiting times may occur before convergence to superdiffusion.

[69] Future observational work is warranted to more definitely describe the type of anomalous diffusion at long times in bed load gravel transport.

5. Conclusion

[70] Our objective in this study was to understand the physical meaning of the anomalous bed particle diffusion observed by *Nikora et al.* [2002] and to relate the time scales of diffusion regimes to the physics of bed load transport. We ran flume experiments to track the dispersion of gravel in bed load transport. At time scales (1/30 to 5 s) corresponding to continuous particle motion, we directly tracked dispersion of continuously moving particles over a fixed rough bed, and related observed superdiffusive transport statistics to particle inertia. Interestingly, recent work probing the limits of classical Brownian motion at the molecular level [*Huang et al.*, 2011] has shown a similar gradual transition from fully correlated (ballistic) motion to random (Brownian) motion, providing a strong analogy for our experiments. From moveable bed experiments, we found an exponential distribution of particle flight times. At time scales (1 to 1000 s) equal to or longer than individual particle flights, we observed heavy-tailed wait times, which suggest that long wait times should be the source of the long-time subdiffusion observed by *Nikora et al.* [2002].

[71] Time scales of anomalous diffusion can be related directly to observable physical quantities. The correlation time scale driving short-time superdiffusion appears to be related to a balance between particle inertia and fluid drag,

though hydrodynamic and boundary effects could also be at work. The mean flight time defines the expected transition from short-time superdiffusion (for continuously moving particles) to long-time subdiffusion (for intermittently moving particles). Finally, the heavy-tailed wait time distribution is related to the distribution of bed scour times. The tail of the wait time distribution in turn should set the scaling of long-time subdiffusion.

[72] Our experiments were designed to replicate dispersion of coarse-grained tracers moving intermittently near the threshold of motion in natural systems. We argue, based on the dynamic similarity of particle velocity distributions to experiments with deeper flows, that the observed dispersion should translate to many other turbulent systems. However, we expect the time scales to be different, especially for different shear stresses and grain sizes. In our experiments, the time scale of particle flights is short enough that expected long-time subdiffusive dynamics are likely to overlap with short-time superdiffusive dynamics driven by correlated particle motions. Finally, as our autoregressive model with grain heterogeneity shows, it is possible for differently sized particles with different mean velocities to produce superdiffusion at time scales significantly beyond the observed correlation time scale. This effect may be further exaggerated for systems with a wider range of grain sizes.

[73] In this paper, we have offered a physically based framework for describing anomalous sediment diffusion. More direct experimental observations are needed to confirm the ideas in this paper, such as the relation between inertial time scale and hydraulic parameters, the dependence of superdiffusion on grain heterogeneity, and the driving physical mechanism behind scour time and wait time variability. Most urgently, experiments tracking particle dispersion from short to long time scales could directly determine transitions among diffusion regimes. We hope that our analyses in this paper can help to set the framework for such experiments.

Appendix A: Derivation of Dispersion Scaling—Inertia Only

[74] Taking the mean and variance of step displacement as $\mu_s = \bar{v}_x \Delta t$ and $\sigma_{s_x}^2 = \sigma_{v_x}^2 \Delta t$, respectively, we define the detrended step random variable as:

$$\tilde{s}_t = s_t - \mu_s. \tag{A1}$$

Similarly, the detrended cumulative displacement is:

$$\tilde{x}_t = x_t - \mu_s t. \tag{A2}$$

[75] We are interested in determining the growth of longitudinal displacement variance, $\sigma_{x,t}^2$. Utilizing the properties of variance, we find:

$$\sigma_{x,t}^2 = \mathrm{Var}(x_t) = \mathrm{Var}(\tilde{x}_t - \mu_s t) = \mathrm{Var}(\tilde{x}_t). \tag{A3}$$

Considering that $\tilde{x}_t = \tilde{x}_{t-1} + \tilde{s}_t$, we can compute $\mathrm{Var}(\tilde{x}_t)$:

$$\mathrm{Var}(\tilde{x}_t) = \mathrm{Var}(\tilde{x}_{t-1} + \tilde{s}_t) = \mathrm{Var}(\tilde{x}_{t-1}) + \mathrm{Var}(\tilde{s}_t) + 2\mathrm{Cov}(\tilde{x}_{t-1}, \tilde{s}_t). \tag{A4}$$

We determine the covariance (Cov) by considering the expected value (E) of successive steps:

$$
\begin{aligned}
\mathrm{Cov}(\tilde{x}_{t-1}, s_t) &= \mathrm{E}[\tilde{x}_{t-1}\tilde{s}_t] \\
&= \mathrm{E}[(\tilde{x}_{t-2} + \tilde{s}_{t-1})\tilde{s}_t] \\
&= \mathrm{E}[\tilde{x}_{t-2}\tilde{s}_t] + \mathrm{E}[\tilde{s}_{t-1}\tilde{s}_t] \\
&= \mathrm{E}[\tilde{x}_{t-3}\tilde{s}_t] + \mathrm{E}[\tilde{s}_{t-2}\tilde{s}_t] + \mathrm{E}[\tilde{s}_{t-1}\tilde{s}_t] \\
&\cdots \\
&= \sum_{i=1}^{t-1} \mathrm{E}[\tilde{s}_{t-i}\tilde{s}_t].
\end{aligned}
\tag{A5}
$$

We can get the expected step products from the autocorrelation function, described in equation (6):

$$\mathrm{E}[\tilde{s}_{t-i}\tilde{s}_t] = \sigma_{s_x}^2 e^{-i/T_c} = \sigma_{s_x}^2 r^i. \tag{A6}$$

[76] Following out the recursive sum in equation (A4), recognizing that $\mathrm{Var}(\tilde{s}_t) = \sigma_{s_x}^2$, and substituting the results of equations (A5) and (A6), we get the displacement variance in terms of t, $\sigma_{s_x}^2$, and r:

$$\sigma_{x,t}^2 = \sigma_{s_x}^2 \left(t + 2\sum_{i=1}^{t-1} r^i(t-i) \right). \tag{A7}$$

The dispersion can be normalized by $\sigma_{s_x}^2$:

$$\sigma_{x*,t}^2 = t + 2\sum_{i=1}^{t-1} r^i(t-i). \tag{A8}$$

Appendix B: Derivation of Dispersion Scaling—Inertia and Grain Heterogeneity

[77] Reframing the model described in equation (15) to include partitioning of velocity variance (equation (17)), we build a new model to incorporate grain heterogeneity:

$$s_t = rs_{t-1} + \mathcal{N}(\mu_\xi, \sigma_{\xi_e}) + \mu_{s_g}. \tag{B1}$$

The noise standard deviation from equation (14) has been modified to account for the velocity partitioning, so that:

$$
\begin{aligned}
\sigma_{\xi_e} &= \sigma_{v_e}\Delta t\sqrt{1-r^2} = \Delta t\sqrt{\left(\sigma_{v_x}^2 - \sigma_{v_g}^2\right)(1-r^2)} \\
&= \sqrt{\left(\sigma_{s_x}^2 - \sigma_{s_g}^2\right)(1-r^2)},
\end{aligned}
\tag{B2}
$$

where $\sigma_{s_x} = \Delta t\sigma_{v_x}$ and $\sigma_{s_g} = \Delta t\sigma_{v_g}$.

[78] The μ_{s_g} term in equation (B1) is a step contribution arising from grain heterogeneity (i.e., the mean deviatoric step of an individual particle due to grain heterogeneity). This value is constant for each grain, but varies among different grains with a normal distribution:

$$\mathrm{P}\left(\mu_{s_g} = x\right) = \mathcal{N}(0, \sigma_{s_g}) = \frac{1}{\sqrt{2\pi\sigma_{s_g}^2}}e^{x^2/\left(2\sigma_{s_g}^2\right)}. \tag{B3}$$

[79] We can relate the dispersion to the expected value of the detrended displacement:

$$\sigma_{x,t}^2 = \text{Var}(\tilde{x}_t) = \text{E}\big[\tilde{x}_t^2\big] - \text{E}[\tilde{x}_t]^2 = \text{E}\big[\tilde{x}_t^2\big]. \tag{B4}$$

To determine the value of $\text{E}\big[\tilde{x}_t^2\big]$, we first condition the expected value on μ_{s_g} as $\text{E}\big[\tilde{x}_t^2|\mu_{s_g}\big]$. We find $\tilde{x}_t|\mu_{s_g}$ by taking the sum of steps:

$$\tilde{x}_t|\mu_{s_g} = \sum_{i=1}^{t} \tilde{s}_i|\mu_{s_g}. \tag{B5}$$

[80] Step sizes depend on previous steps. Taking $\tilde{s}_1$ as a random variable for the first step and $\tilde{\xi}_i$ as the random (detrended) noise term at the ith time step, the steps follow the pattern:

$$\tilde{s}_1|\mu_{s_g} = \tilde{s}_1,$$
$$\tilde{s}_2|\mu_{s_g} = r\tilde{s}_1 + \big(\tilde{\xi}_2 + \mu_{s_g}\big),$$
$$\tilde{s}_3|\mu_{s_g} = r^2\tilde{s}_1 + r\big(\tilde{\xi}_2 + \mu_{s_g}\big) + \big(\tilde{\xi}_3 + \mu_{s_g}\big),$$
$$\dots$$
$$\tilde{s}_i|\mu_{s_g} = r^{i-1}\tilde{s}_1 + r^{i-2}\big(\tilde{\xi}_2 + \mu_{s_g}\big) + r^{i-3}\big(\tilde{\xi}_3 + \mu_{s_g}\big) + \dots$$
$$+ r\big(\tilde{\xi}_{i-1} + \mu_{s_g}\big) + \big(\tilde{\xi}_i + \mu_{s_g}\big). \tag{B6}$$

The sum of the steps is then:

$$\tilde{x}_t|\mu_{s_g} = \sum_{i=0}^{t-1} r^i\tilde{s}_1 + \sum_{i=0}^{t-2} r^i\big(\tilde{\xi}_2 + \mu_{s_g}\big) + \sum_{i=0}^{t-3} r^i\big(\tilde{\xi}_3 + \mu_{s_g}\big)$$
$$+ \dots + r^0\big(\tilde{\xi}_t + \mu_{s_g}\big)$$
$$= \left(\frac{1-r^t}{1-r}\right)\tilde{s}_1 + \left(\frac{1-r^{t-1}}{1-r}\right)\big(\tilde{\xi}_2 + \mu_{s_g}\big)$$
$$+ \left(\frac{1-r^{t-2}}{1-r}\right)\big(\tilde{\xi}_3 + \mu_{s_g}\big) + \dots + \big(\tilde{\xi}_t + \mu_{s_g}\big)$$
$$= \left(\frac{1}{1-r}\right)\left[(1-r^t)\tilde{s}_1 + \sum_{i=1}^{t-1}(1-r^i)\big(\tilde{\xi}_{t-i+1} + \mu_{s_g}\big)\right]. \tag{B7}$$

Taking the square, we get:

$$\tilde{x}_t^2|\mu_{s_g} = \left(\frac{1}{1-r}\right)^2\left[(1-r^t)^2\tilde{s}_1^2 + \sum_{i=1}^{t-1}(1-r^i)^2\big(\tilde{\xi}_{t-i+1} + \mu_{s_g}\big)^2\right.$$
$$+ \sum_{\substack{i=1,j=1 \\ i\neq j}}^{t-1}(1-r^i)(1-r^j)\big(\tilde{\xi}_{t-i+1} + \mu_{s_g}\big)\big(\tilde{\xi}_{t-j+1} + \mu_{s_g}\big)$$
$$\left. + 2(1-r^t)\tilde{s}_1\left(\sum_{i=1}^{t-1}(1-r^i)\big(\tilde{\xi}_{t-i+1} + \mu_{s_g}\big)\right)\right]. \tag{B8}$$

[81] To determine the expected value of $\tilde{x}_t^2|\mu_{s_g}$, we take the expected values of the random variables, noting that $\tilde{s}_1$ and all of the $\tilde{\xi}_i$'s are independent:

$$\text{E}\big[\tilde{x}_t^2|\mu_{s_g}\big] = \left(\frac{1}{1-r}\right)^2\left[(1-r^t)^2\text{E}[\tilde{s}_1^2] + \sum_{i=1}^{t-1}(1-r^i)^2\left(\text{E}\big[\tilde{\xi}_{t-i+1}^2\big]\right.\right.$$
$$+ 2\text{E}\big[\tilde{\xi}_{t-i+1}\big]\mu_{s_g} + \mu_{s_g}^2\Big) + \sum_{\substack{i=1,j=1 \\ i\neq j}}^{t-1}(1-r^i)(1-r^j)$$
$$\cdot\left(\text{E}\big[\tilde{\xi}_{t-i+1}\tilde{\xi}_{t-j+1}\big] + \text{E}\big[\tilde{\xi}_{t-i+1}\big]\mu_{s_g} + \text{E}\big[\tilde{\xi}_{t-j+1}\big]\mu_{s_g} + \mu_{s_g}^2\right)$$
$$\left. + 2(1-r^t)\text{E}[\tilde{s}_1]\left(\sum_{i=1}^{t-1}(1-r^i)\left(\text{E}\big[\tilde{\xi}_{t-i+1}\big] + \mu_{s_g}\right)\right)\right]. \tag{B9}$$

The expected values of the random variables are: $\text{E}[\tilde{s}_1] = 0$, $\text{E}[\tilde{\xi}_i] = 0$, $\text{E}[\tilde{s}_1^2] = \sigma_s^2$, and $\text{E}\big[\tilde{\xi}_i^2\big] = \sigma_{\tilde{\xi}_e}^2$. Thus, we can simplify:

$$\text{E}\big[\tilde{x}_t^2|\mu_{s_g}\big] = \left(\frac{1}{1-r}\right)^2\left[\sigma_s^2(1-r^t)^2 + \big(\sigma_{\tilde{\xi}_e}^2 + \mu_{s_g}^2\big)\sum_{i=1}^{t-1}(1-r^i)^2\right.$$
$$\left. + \mu_{s_g}^2\sum_{\substack{i=1,j=1 \\ i\neq j}}^{t-1}(1-r^i)(1-r^j)\right]$$
$$= \left(\frac{1}{1-r}\right)^2\left[\sigma_s^2(1-r^t)^2 + \sigma_{\tilde{\xi}}^2\sum_{i=1}^{t-1}(1-r^i)^2\right.$$
$$\left. + \mu_{s_g}^2\left(\sum_{i=1}^{t-1}1-r^i\right)^2\right]. \tag{B10}$$

Recognizing from equation (B2) that $\sigma_{\tilde{\xi}_e} = \sqrt{\big(\sigma_{s_x}^2 - \sigma_{s_g}^2\big)(1-r^2)}$,

$$\text{E}\big[\tilde{x}_t^2|\mu_{s_g}\big] = \left(\frac{1}{1-r}\right)^2\left[\sigma_s^2(1-r^t)^2 + \big(\sigma_s^2 - \sigma_{s_g}^2\big)(1-r^2)\right.$$
$$\left. \cdot\sum_{i=1}^{t-1}(1-r^i)^2 + \mu_{s_g}^2\left(\sum_{i=1}^{t-1}1-r^i\right)^2\right]. \tag{B11}$$

[82] Defining the constants A and B:

$$A = \left(\frac{1}{1-r}\right)^2\left[\sigma_s^2(1-r^t)^2 + \big(\sigma_s^2 - \sigma_{s_g}^2\big)(1-r^2)\sum_{i=1}^{t-1}(1-r^i)^2\right], \tag{B12}$$

$$B = \left(\frac{1}{1-r}\right)^2\left(\sum_{i=1}^{t-1}1-r^i\right)^2. \tag{B13}$$

We can rewrite equation (B11):

$$\mathrm{E}\left[\tilde{x}_t^2 | \mu_{s_g}\right] = A + B\mu_{s_g}^2. \tag{B14}$$

Now, utilizing the law of total probability,

$$\mathrm{E}\left[\tilde{x}_t^2\right] = \int_{-\infty}^{\infty} \mathrm{E}\left[\tilde{x}_t^2 | \mu_{s_g}\right] P\left(\mu_{s_g} = x\right) \mathrm{d}x. \tag{B15}$$

Substituting equations (B3) and (B11) into equation (B15), we get:

$$\mathrm{E}\left[\tilde{x}_t^2\right] = \int_{-\infty}^{\infty} \left(A + Bx^2\right) \frac{1}{\sqrt{2\pi\sigma_{s_g}^2}} e^{x^2/\left(2\sigma_{s_g}^2\right)} \mathrm{d}x. \tag{B16}$$

Integrating, we recover the dispersion scaling with time:

$$\sigma_{x,t}^2 = \mathrm{E}\left[\tilde{x}_t^2\right] = A + B\sigma_{s_g}^2, \tag{B17}$$

with A and B from equations (B12) and (B13). The dispersion depends on the correlation time, expressed through r, and the relative contributions of $\sigma_{s_g}^2$ and σ_s^2 to velocity variability.

Appendix C: Derivation of Velocity Variance Scaling

[83]   Taking the number of time steps, $t = \delta t/\Delta t$, where δt is the time interval and Δt is the time step of the autoregressive model, the expected scaling of velocity variance, $\sigma_{v_x}^2$, for completely uncorrelated motion by the Central Limit Theorem (CLT) is:

$$\sigma_{v_x,\mathrm{CLT}}^2(t) = \frac{\sigma_s^2}{t}, \tag{C1}$$

where σ_s^2 is the velocity variance for $t = 1$.

[84]   However, since velocities are correlated by inertia, we expect $\sigma_{v_x}^2$ to decrease more slowly than predicted by the CLT. Here, velocity variance scaling is just the displacement variance scaling computed in equation (16) divided by time:

$$\sigma_{v_x,\mathrm{inertia}}^2(t) = \frac{\sigma_{x,t}^2}{t} = \sigma_{s_x}^2\left(1 + \frac{2}{t}\sum_{i=1}^{t-1} r^i(t-i)\right). \tag{C2}$$

[85]   When taking into account grain heterogeneity, the velocity variance should no longer converge to zero, but instead should converge to $\sigma_{v_g}^2$. Thus, we modify equation (C2) to include this fact:

$$\sigma_{v_x,\mathrm{inertia,grain}}^2(t) = \sigma_{s_e}^2\left(1 + \frac{2}{t}\sum_{i=1}^{t-1} r^i(t-i)\right) + \sigma_{v_g}^2. \tag{C3}$$

References

Abbott, J., and J. Francis (1977), Saltation and suspension trajectories of solid grains in a water stream, *Philos. Trans. R. Soc. London A*, *284*(1321), 225–254, doi:10.1098/rsta.1977.0009.
Ancey, C. (2010), Stochastic modeling in sediment dynamics: Exner equation for planar bed incipient bed load transport conditions, *J. Geophys. Res.*, *115*, F00A11, doi:10.1029/2009JF001260.
Ancey, C., F. Bigillon, P. Frey, J. Lanier, and R. Ducret (2002), Saltating motion of a bead in a rapid water stream, *Phys. Rev. E*, *66*(3), 036306, doi:10.1103/PhysRevE.66.036306.
Ancey, C., F. Bigillon, P. Frey, and R. Ducret (2003), Rolling motion of a bead in a rapid water stream, *Phys. Rev. E.*, *67*(1), 011303, doi:10.1103/PhysRevE.67.011303.
Ancey, C., A. Davison, T. Bohm, M. Jodeau, and P. Frey (2008), Entrainment and motion of coarse particles in a shallow water stream down a steep slope, *J. Fluid Mech.*, *595*, 83–114, doi:10.1017/S0022112007008774.
Andrews, E. D. (1983), Entrainment of gravel from naturally sorted riverbed material, *Geol. Soc. Am. Bull.*, *94*(10), 1225–1231.
Bagnold, R. A. (1966), An approach to the sediment transport problem from general physics, *U.S. Geol. Surv. Prof. Pap.*, *422-I*, 37 pp.
Bagnold, R. A. (1973), The nature of saltation and of "bed-load" transport in water, *Proc. R. Soc. London, Ser. A*, *332*(1591), 473–504, doi:10.1098/rspa.1973.0038.
Bouchaud, J., and A. Georges (1990), Anomalous diffusion in disordered media: Statistical mechanisms, models and physical applications, *Phys. Rep.*, *195*(4–5), 127–293, doi:10.1016/0370-1573(90)90099-N.
Bradley, D. N., G. E. Tucker, and D. A. Benson (2010), Fractional dispersion in a sand bed river, *J. Geophys. Res.*, *115*, F00A09, doi:10.1029/2009JF001268.
Bridge, J. S., and D. F. Dominic (1984), Bed load grain velocities and sediment transport rates, *Water Resour. Res.*, *20*(4), 476–490, doi:10.1029/WR020i004p00476.
Buffin-Belanger, T., and A. G. Roy (1998), Effects of a pebble cluster on the turbulent structure of a depth-limited flow in a gravel-bed river, *Geomorphology*, *25*(3-4), 249–267, doi:10.1016/S0169-555X(98)00062-2.
Buffington, J. M., and D. R. Montgomery (1997), A systematic analysis of eight decades of incipient motion studies, with special reference to gravel-bedded rivers, *Water Resour. Res.*, *33*(8), 1993–2029, doi:10.1029/96WR03190.
Buffington, J. M., W. E. Dietrich, and J. W. Kirchner (1992), Friction angle measurements on a naturally formed gravel streambed: Implications for critical boundary shear stress, *Water Resour. Res.*, *28*(2), 411–425, doi:10.1029/91WR02529.
Carreras, B. A., V. E. Lynch, D. E. Newman, and G. M. Zaslavsky (1999), Anomalous diffusion in a running sandpile model, *Phys. Rev. E.*, *60*(4), 4770–4778, doi:10.1103/PhysRevE.60.4770.
Chacho, E., W. Emmett, and R. Burrows (1994), Monitoring gravel movement using radio transmitters, in *Hydraulic Engineering '94*, edited by G. V. Cotroneo and R. R. Rumer, pp. 785–789, Am. Soc. of Civ. Eng., Buffalo, N. Y.
Chin, A. (2002), The periodic nature of step-pool mountain streams, *Am. J. Sci.*, *302*(2), 144–167, doi:10.2475/ajs.302.2.144.
Chin, A., and E. Wohl (2005), Toward a theory for step pools in stream channels, *Prog. Phys. Geogr.*, *29*(3), 275–296, doi:10.1191/0309133305pp449ra.
Church, M., and A. Zimmermann (2007), Form and stability of step-pool channels: Research progress, *Water Resour. Res.*, *43*, W03415, doi:10.1029/2006WR005037.
Clercx, H. J. H., and P. P. J. M. Schram (1992), Brownian particles in shear flow and harmonic potentials: A study of long-time tails, *Phys. Rev. A*, *46*(4), 1942–1950, doi:10.1103/PhysRevA.46.1942.
Comiti, F., D. Cadol, and E. Wohl (2009), Flow regimes, bed morphology, and flow resistance in self-formed step-pool channels, *Water Resour. Res.*, *45*, W04424, doi:10.1029/2008WR007259.
Dade, W., and P. Friend (1998), Grain-size, sediment-transport regime, and channel slope in alluvial rivers, *J. Geol.*, *106*(6), 661–676, doi:10.1086/516052.
Drake, T., R. Shreve, W. Dietrich, P. Whiting, and L. Leopold (1988), Bedload transport of fine gravel observed by motion-picture photography, *J. Fluid Mech.*, *192*, 193–217, doi:10.1017/S0022112088001831.

Einstein, H. A. (1950), The bed-load function for sediment transportation in open channel flows, *Tech. Bull. 1026*, U.S. Dep. of Agric., Washington, D. C.

Einstein, H. A. (1972), Bed load transport as a probability problem, in *Sedimentation Symposium to Honor Professor H. A. Einstein*, edited by H. W. Shen, pp. C1–C105, Fort Collins, Colo.

Elghobashi, S., and G. C. Truesdell (1992), Direct simulation of particle dispersion in a decaying isotropic turbulence, *J. Fluid. Mech.*, *242*, 655–700, doi:10.1017/S0022112092002532.

Ergenzinger, P., K. Schmidt, and R. Busskamp (1989), The pebble transmitter system (PETS): First results of a technique for studying coarse material erosion, transport and deposition, *Z. Geomorphol.*, *33*, 503–508.

Fenton, J., and J. Abbott (1977), Initial movement of grains on a stream bed: The effect of relative protrusion, *Proc. R. Soc. London, Ser. A*, *352*(1671), 523–537, doi:10.1098/rspa.1977.0014.

Ferguson, R., and M. Church (2004), A simple universal equation for grain settling velocity, *J. Sediment. Res.*, *74*(6), 933–937, doi:10.1306/051204740933.

Fernandez Luque, R. (1974), Erosion and transport of bed-load sediment, PhD thesis, Delft Univ. of Tech., Delft, Netherlands.

Fernandez Luque, R., and R. Van Beek (1976), Erosion and transport of bed-load sediment, *J. Hydraul. Res.*, *14*(2), 127–144.

Foufoula-Georgiou, E., and C. Stark (2010), Introduction to special section on Stochastic Transport and Emergent Scaling on Earth's Surface: Rethinking geomorphic transport—Stochastic theories, broad scales of motion, and nonlocality, *J. Geophys. Res.*, *115*, F00A01, doi:10.1029/2010JF001661.

Foufoula-Georgiou, E., V. Ganti, and W. E. Dietrich (2010), A nonlocal theory of sediment transport on hillslopes, *J. Geophys. Res.*, *115*, F00A16, doi:10.1029/2009JF001280.

Francis, J. R. D. (1973), Experiments on the motion of solitary grains along the bed of a water-stream, *Proc. R. Soc. London, Ser. A*, *332*(1591), 443–471, doi:10.1098/rspa.1973.0037.

Fredsøe, J., and F. Engelund (1975), Bed configurations in open and closed alluvial channels, *Ser. Pap. 8*, 39 pp., Inst. of Hydrodyn. and Hydraul. Eng., Copenhagen.

Ganti, V., A. Singh, P. Passalacqua, and E. Foufoula-Georgiou (2009), Subordinated Brownian motion model for sediment transport, *Phys. Rev. E.*, *80*(1), 011111, doi:10.1103/PhysRevE.80.011111.

Gomez, B., and J. D. Phillips (1999), Deterministic uncertainty in bed load transport, *J. Hydraul. Eng.*, *125*(3), 305–308, doi:10.1061/(ASCE)0733-9429(1999)125:3(305).

Granger, D. E., J. W. Kirchner, and R. Finkel (1996), Spatially averaged long-term erosion rates measured from in situ-produced cosmogenic nuclides in alluvial sediment, *J. Geol.*, *104*(3), 249–257.

Grant, G. E., F. J. Swanson, and M. G. Wolman (1990), Pattern and origin of stepped-bed morphology in high-gradient streams, Western Cascades, Oregon, *Geol. Soc. Am. Bull.*, *102*(3), 340–352.

Habersack, H. M. (2001), Radio-tracking gravel particles in a large braided river in New Zealand: A field test of the stochastic theory of bed load transport proposed by Einstein, *Hydrol. Processes*, *15*(3), 377–391, doi:10.1002/hyp.147.

Hassan, M. A., M. Church, and A. P. Schick (1991), Distance of movement of coarse particles in gravel bed streams, *Water Resour. Res.*, *27*(4), 503–511, doi:10.1029/90WR02762.

Hill, K. M., L. DellAngelo, and M. M. Meerschaert (2010), Heavy-tailed travel distance in gravel bed transport: An exploratory enquiry, *J. Geophys. Res.*, *115*, F00A14, doi:10.1029/2009JF001276.

Hu, C., and Y. Hui (1996a), Bed-load transport. II: Stochastic characteristics, *J. Hydraul. Eng.*, *122*(5), 255–261, doi:10.1061/(ASCE)0733-9429(1996)122:5(255).

Hu, C., and Y. Hui (1996b), Bed-load transport. I: Mechanical characteristics, *J. Hydraul. Eng.*, *122*(5), 245–254, doi:10.1061/(ASCE)0733-9429(1996)122:5(245).

Huang, R., I. Chavez, K. M. Taute, B. Lukic, S. Jeney, M. G. Raizen, and E. Florin (2011), Direct observation of the full transition from ballistic to diffusive Brownian motion in a liquid, *Nat. Phys.*, *7*, 576–580, doi:10.1038/nphys1953.

Kumar, N., U. Harbola, and K. Lindenberg (2010), Memory-induced anomalous dynamics: Emergence of diffusion, subdiffusion, and superdiffusion from a single random walk model, *Phys. Rev. E*, *82*(2), 021101, doi:10.1103/PhysRevE.82.021101.

Lajeunesse, E., L. Malverti, and F. Charru (2010), Bed load transport in turbulent flow at the grain scale: Experiments and modeling, *J. Geophys. Res.*, *115*, F04001, doi:10.1029/2009JF001628.

Lamarre, H., and A. G. Roy (2008), The role of morphology on the displacement of particles in a step-pool river system, *Geomorphology*, *99*, 270–279, doi:10.1016/j.geomorph.2007.11.005.

Lamarre, H., B. MacVicar, and A. G. Roy (2005), Using passive integrated transponder (PIT) tags to investigate sediment transport in gravel-bed rivers, *J. Sediment. Res.*, *75*(4), 736–741, doi:10.2110/jsr.2005.059.

Lee, H., and I. Hsu (1994), Investigation of saltating particle motions, *J. Hydraul. Eng.*, *120*(7), 831–845, doi:10.1061/(ASCE)0733-9429(1994)120:7(831).

Lenzi, M. A. (2001), Step-pool evolution in the Rio Cordon, northeastern Italy, *Earth Surf. Processes Landforms*, *26*(9), 991–1008, doi:10.1002/esp.239.

Li, T., S. Kheifets, D. Medellin, and M. G. Raizen (2010), Measurement of the instantaneous velocity of a Brownian particle, *Science*, *328*(5986), 1673–1675, doi:10.1126/science.1189403.

Lisle, I. G., C. W. Rose, W. L. Hogarth, P. B. Hairsine, G. C. Sander, and J. Y. Parlange (1998), Stochastic sediment transport in soil erosion, *J. Hydrol.*, *204*(1–4), 217–230, doi:10.1016/S0022-1694(97)00123-6.

Magdziarz, M., A. Weron, K. Burnecki, and J. Klafter (2009), Fractional Brownian motion versus the continuous-time random walk: A simple test for subdiffusive dynamics, *Phys. Rev. Lett.*, *103*(18), 180602, doi:10.1103/PhysRevLett.103.180602.

Mandelbrot, B. B., and J. W. V. Ness (1968), Fractional Brownian motions, fractional noises and applications, *SIAM Rev.*, *10*(4), 422–437.

Marchesoni, F., and A. Taloni (2006), Subdiffusion and long-time anticorrelations in a stochastic single file, *Phys. Rev. Lett.*, *97*(10), 106101, doi:10.1103/PhysRevLett.97.106101.

McNamara, J. P., and C. Borden (2004), Observations on the movement of coarse gravel using implanted motion-sensing radio transmitters, *Hydrol. Processes*, *18*(10), 1871–1884, doi:10.1002/hyp.1453.

Meland, N., and J. O. Norrman (1966), Transport velocities of single particles in bed-load motion, *Geogr. Ann. A*, *48*(4), 165–182, doi:10.2307/520500.

Metzler, R., and J. Klafter (2000), The random walk's guide to anomalous diffusion: A fractional dynamics approach, *Phys. Rep.*, *339*(1), 1–77, doi:10.1016/S0370-1573(00)00070-3.

Middleton, G., and J. Southard (1977), *Mechanics of Sediment Movement*, Soc. of Econ. Paleontol. and Mineral., Binghamton, N. Y.

Montgomery, D. R., and J. M. Buffington (1997), Channel-reach morphology in mountain drainage basins, *Geol. Soc. Am. Bull.*, *109*(5), 596–611.

Mueller, E. R., and J. Pitlick (2005), Morphologically based model of bed load transport capacity in a headwater stream, *J. Geophys. Res.*, *110*, F02016, doi:10.1029/2003JF000117.

Nakagawa, H., and T. Tsujimoto (1980), A stochastic model for bed load transport and its applications to alluvial phenomena, in *Application of Stochastic Processes in Sediment Transport*, edited by H. W. Shen and H. Kikkawa, pp. 11-1–11-54, Water Resour., Littleton, Colo.

Nelson, J. M., R. L. Shreve, S. R. McLean, and T. G. Drake (1995), Role of near-bed turbulence structure in bed load transport and bed form mechanics, *Water Resour. Res.*, *31*(8), 2071–2086, doi:10.1029/95WR00976.

Nikora, V., and D. Goring (2001), Spatially averaged open-channel flow over rough bed, *J. Hydraul. Eng.*, *127*(2), 123–133, doi:10.1061/(ASCE)0733-9429(2001)127:2(123).

Nikora, V., H. H. Habersack, T. Huber, and I. McEwan (2002), On bed particle diffusion in gravel bed flows under weak bed load transport, *Water Resour. Res.*, *38*(6), 1081, doi:10.1029/2001WR000513.

Nino, Y., M. Garcia, and L. Ayala (1994), Gravel saltation: 1. Experiments, *Water Resour. Res.*, *30*(6), 1907–1914, doi:10.1029/94WR00533.

Nuyts, J. (2010), Inference about the tail of a distribution: Improvement on the Hill estimator, *Int. J. Math. Math. Sci.*, *2010*, 924013, doi:10.1155/2010/924013.

Parker, G. (1978), Self-formed straight rivers with equilibrium banks and mobile bed. Part 2. The gravel river, *J. Fluid Mech.*, *89*(1), 127–146, doi:10.1017/S0022112078002505.

Parker, G., P. R. Wilcock, C. Paola, W. E. Dietrich, and J. Pitlick (2007), Physical basis for quasi-universal relations describing bankfull hydraulic geometry of single-thread gravel bed rivers, *J. Geophys. Res.*, *112*, F04005, doi:10.1029/2006JF000549.

Phillips, J. D. (2006), Deterministic chaos and historical geomorphology: A review and look forward, *Geomorphology*, *76*(1–2), 109–121, doi:10.1016/j.geomorph.2005.10.004.

Reid, I., L. E. Frostick, and J. T. Layman (1985), The incidence and nature of bedload transport during flood flows in coarse-grained alluvial channels, *Earth Surf. Proc. Land.*, *10*(1), 33–44, doi:10.1002/esp.3290100107.

Sayre, W., and D. Hubbell (1965), Transport and dispersion of labeled bed material, North Loup River, Nebraska, *U.S. Geol. Surv. Prof. Pap.*, *433-C*, 48 pp.

Schmidt, K., and P. Ergenzinger (1992), Bedload entrainment, travel lengths, step lengths, rest periods–Studied with passive (iron, magnetic)

and active (radio) tracer techniques, *Earth Surf. Processes Landforms, 17* (2), 147–165, doi:10.1002/esp.3290170204.

Schumer, R., M. M. Meerschaert, and B. Baeumer (2009), Fractional advection-dispersion equations for modeling transport at the earth surface, *J. Geophys. Res., 114*, F00A07, doi:10.1029/2008JF001246.

Sekine, M., and H. Kikkawa (1992), Mechanics of saltating grains. II, *J. Hydraul. Eng., 118*(4), 536–558, doi:10.1061/(ASCE)0733-9429(1992) 118:4(536).

Seminara, G., L. Solari, and G. Parker (2002), Bed load at low Shields stress on arbitrarily sloping beds: Failure of the Bagnold hypothesis, *Water Resour. Res., 38*(11), 1249, doi:10.1029/2001WR000681.

Singh, A., K. Fienberg, D. J. Jerolmack, J. Marr, and E. Foufoula-Georgiou (2009), Experimental evidence for statistical scaling and intermittency in sediment transport rates, *J. Geophys. Res., 114*, F01025, doi:10.1029/ 2007JF000963.

Snyder, W. H., and J. L. Lumley (1971), Some measurements of particle velocity autocorrelation functions in a turbulent flow, *J. Fluid Mech., 48*(1), 41–71, doi:10.1017/S0022112071001460.

Stark, C. P., E. Foufoula-Georgiou, and V. Ganti (2009), A nonlocal theory of sediment buffering and bedrock channel evolution, *J. Geophys. Res., 114*, F01029, doi:10.1029/2008JF000981.

Tucker, G. E., and D. N. Bradley (2010), Trouble with diffusion: Reassessing hillslope erosion laws with a particle-based model, *J. Geophys. Res., 115*, F00A10, doi:10.1029/2009JF001264.

van Rijn, L. C. (1984), Sediment transport, Part I: Bed load transport, *J. Hydraul. Eng., 110*(10), 1431–1456, doi:10.1061/(ASCE)0733-9429(1984)110:10(1431).

Voller, V. R., and C. Paola (2010), Can anomalous diffusion describe depositional fluvial profiles?, *J. Geophys. Res., 115*, F00A13, doi:10.1029/2009JF001278.

Weeks, E. R., J. S. Urbach, and H. L. Swinney (1996), Anomalous diffusion in asymmetric random walks with a quasi-geostrophic flow example, *Physica D, 97*(1–3), 291–310, doi:10.1016/0167-2789(96)00082-6.

Whittaker, J., and M. Jaeggi (1982), Origin of step-pool systems in mountain streams, *J. Hydraul. Div. Am. Soc. Civ. Eng., 108*(6), 758–773.

Wiberg, P. L., and J. D. Smith (1989), Model for calculating bed load transport of sediment, *J. Hydraul. Eng., 115*(1), 101–123, doi:10.1061/ (ASCE)0733-9429(1989)115:1(101).

Wilcock, P. R. (1997), Entrainment, displacement and transport of tracer gravels, *Earth Surf. Processes Landforms, 22*(12), 1125–1138.

Wilcock, P. R. (1998), Two-fraction model of initial sediment motion in gravel-bed rivers, *Science, 280*(5362), 410–412, doi:10.1126/science. 280.5362.410.

Willenbring, J. K., and F. von Blanckenburg (2010), Meteoric cosmogenic beryllium-10 adsorbed to river sediment and soil: Applications for Earth-surface dynamics, *Earth Sci. Rev., 98*, 105–122, doi:10.1016/j.earscirev. 2009.10.008.

Wong, M., G. Parker, P. DeVries, T. M. Brown, and S. J. Burges (2007), Experiments on dispersion of tracer stones under lower-regime plane-bed equilibrium bed load transport, *Water Resour. Res., 43*, W03440, doi:10.1029/2006WR005172.

Zimmermann, A., and M. Church (2001), Channel morphology, gradient profiles and bed stresses during flood in a step-pool channel, *Geomorphology, 40*(3–4), 311–327, doi:10.1016/S0169-555X(01)00057-5.

D. J. Jerolmack and R. L. Martin, Department of Earth and Environmental Science, University of Pennsylvania, Philadelphia, PA 19104, USA. (sediment@sas.upenn.edu; raleighm@sas.upenn.edu)

R. Schumer, Division of Hydrologic Sciences, Desert Research Institute, Reno, NV 89512, USA. (rina@dri.edu)